REPORT No. 361

EXPERIMENTAL DETERMINATION OF JET BOUNDARY CORRECTIONS FOR AIRFOIL TESTS IN FOUR OPEN WIND TUNNEL JETS OF DIFFERENT SHAPES

By MONTGOMERY KNIGHT and THOMAS A. HARRIS
Langley Memorial Aeronautical Laboratory

REPORT No. 361

EXPERIMENTAL DETERMINATION OF JET BOUNDARY CORRECTIONS FOR AIRFOIL TESTS IN FOUR OPEN WIND TUNNEL JETS OF DIFFERENT SHAPES

By MONTGOMERY KNIGHT and THOMAS A. HARRIS

SUMMARY

This experimental investigation was conducted primarily for the purpose of obtaining a method of correcting to free air conditions the results of airfoil force tests in four open wind tunnel jets of different shapes. Tests were also made to determine whether the jet boundaries had any appreciable effect on the pitching moments of a complete airplane model. The investigation was conducted in the Atmospheric Wind Tunnel of the Langley Memorial Aeronautical Laboratory.

The method of obtaining the airfoil corrections utilized the results of force tests made in each jet on three similar monoplane airfoil set-ups of different sizes. The data from the tests in one of the jets which was circular were extrapolated to the condition of infinite air space, and the results were found to agree with those obtained by means of Prandtl's theoretical method of correction. On this basis corrections were then obtained for all the other airfoil tests.

Satisfactory corrections for the effect of the boundaries of the various jets were obtained for all the airfoils tested, the span of the largest being 0.75 of the jet width. The corrections for angle of attack were, in general, larger than those for drag. The boundaries had no appreciable effect on the pitching moments of either the airfoils or the complete airplane model. Increasing turbulence appeared to increase the minimum drag and maximum lift and to decrease the pitching moment.

INTRODUCTION

The results of tests on models in wind tunnels are not directly applicable to airplanes in flight, because tunnel conditions modify the airflow. Some causes of the discrepancies are known, and corrections have been derived which bring model and full scale results into better agreement. These corrections depend upon the particular tunnel in which the model is tested, and are made necessary chiefly by the effects of scale, turbulence, and jet boundaries.

The scale effect is due to the difference between the nature of the air flow around the model in the tunnel and that around the airplane in flight. This difference is usually expressed in terms of the Reynolds Number, which, for air under ordinary conditions, is proportional to the air speed and the size of the object. Although a considerable amount of data is available on model tests at various Reynolds Numbers, no general corrections for scale effect have been obtained, because of the erratic variation of the forces with changes in scale. A discussion of scale effect will be found in Reference 1.

In general, no two wind tunnels have the same amount of turbulence. The information on this effect is very limited and no corrections have thus far been derived. Some of the most recent work that has been done on this problem is described in References 2 and 3.

Jet boundary corrections are necessary, since, due to the limited cross section of the wind tunnel jet, the model causes a deflection of the air which is different from that caused by the airplane in flight. This correction depends upon the relative size of the model and jet and upon the jet shape. In addition, the correction is not the same for open and closed jets. Prandtl (Reference 4) has derived a theoretical correction for this effect in open and closed jets of circular cross section, and an experimental check has been made (Reference 5). Theoretical corrections for various shapes of closed rectangular jets also have been obtained by Glauert, as given in Reference 6.

The cross-sectional area of the jet determines in a large measure the cost and size of a wind tunnel structure, as well as the power required to operate it. Consequently, it is desirable to keep the jet area as small as possible, consistent with obtaining a given Reynolds Number. A way of reducing this area for a given model span is to decrease the jet depth, the width remaining the same, thus departing from the circular or square jets that have been common hitherto. The area may be reduced further by rounding the sides of the jet. Because of the ease of accessibility of the model, an open-jet tunnel is desirable.

Most of the more recently built tunnels have open jets, but no corrections for jet boundary effect in open-throat tunnels of other than circular cross section have been hitherto available.

This experimental investigation was conducted for the purpose of obtaining the jet boundary corrections for monoplane airfoils in four shapes of open jets. These shapes as shown in Figure 1 were as follows:

1. Circular.
2. $\sqrt{2}$ to 1 rectangular.
3. $\sqrt{2}$ to 1 with semicircular sides.
4. 2 to 1 with semicircular sides.

The method used in determining these corrections consisted of plotting the results of force tests made in the circular jet on three similar airfoil set-ups of different sizes. The forces corresponding to free air conditions were then obtained by extrapolation, and the corrections for the tests in the other three jets were derived on this basis.

In order to obtain information on the effect of jet boundaries on the pitching moments of a relatively

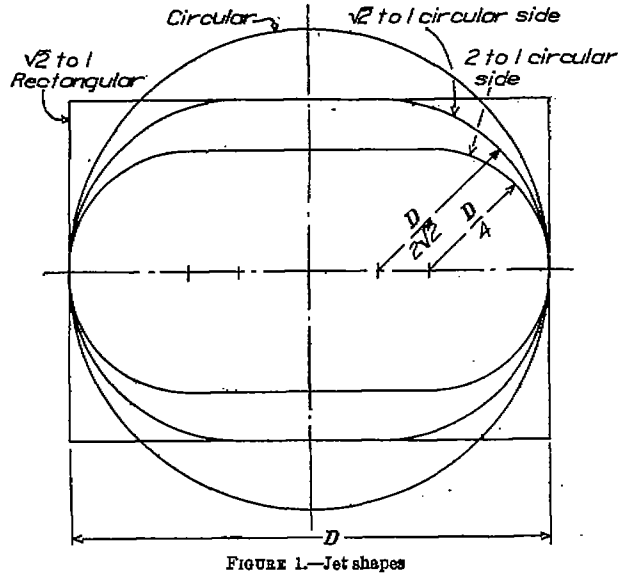

FIGURE 1.—Jet shapes

large airplane model equipped with fuselage and tail surfaces, additional tests were made in each jet on a complete model of a seaplane.

In these tests, which were made in the Atmospheric Wind Tunnel of the Langley Memorial Aeronautical Laboratory, the various jets were produced by replacing the regular closed throat of this tunnel with the proper entrance and exit cones surrounded by a rectangular box to simulate the test chamber. Figure 2 is a general cross-sectional view of the tunnel arrangement with the circular cones in place.

MODELS AND APPARATUS

The details and dimensions of the four jets and pairs of entrance and exit cones are shown in Figure 3. The slots shown in the exit cone were to prevent organ pipe pulsation as explained in Reference 7. Instead of the customary exit cone flare, a cross-tunnel wall was built flush with the end of the exit cone providing an annular space around the cone, preliminary experiments on a model of a wind tunnel having shown that satisfactory flow could be obtained with this construction. This arrangement was used as shown in Figure 3, because of its simplicity of construction. The slots shown around the outer edge of the wall allowed the spillage air to circulate. The cones were constructed of one-sixteenth inch sheet iron. To insure the proper shape, the mouth of each entrance cone was made of wood. A wooden test chamber was built symmetrically about the center line of each jet, and was proportional to the jet dimensions, as shown in Figure 3. The test chambers were all of the same length and width, while the height was in each case double the height of the particular jet.

The three models used to determine the correction factors were rectangular Clark Y airfoils, built of laminated mahogany. The chord lengths were 3, 4, and 5 inches, and in each case the aspect ratio was 5. The spans of the airfoils were, respectively, 0.45, 0.60, and 0.75 of the width of the jets. Expanded profile curves (Figures 4, 5, and 6) show the specified and average measured ordinates of these airfoils. The measured ordinates were obtained by taking the mean values from measurements made at a quarter of the span from each end of the airfoil. These measurements were made with a dividing engine.

The complete airplane model tested was a one-twelfth scale replica of the Navy T. S. seaplane. The span of the model was 0.75 of the width of the jets.

The three airfoil setups in each jet were made as nearly similar as possible in order that the results might be comparable without corrections for support drag and interference. This was accomplished by the use of similar wing skids, lugs, links, wires, and wire shields, all dimensions of which were proportional to the chords of the airfoils as shown in Figure 7. Setups of the 5-inch chord airfoil in the various jets are shown in Figures 8, 9, 10, and 11, and of the seaplane in the 2 to 1 jet in Figure 12.

The wire balance used in these tests to measure the forces on the models was similar to the one described in Reference 8.

In the turbulence tests, described later, the small end of the rectangular entrance cone was covered with chicken wire. Figure 13 is a photograph of this wire showing the size of the mesh.

A standard Prandtl Pitot tube was used for making the initial dynamic pressure surveys. During the force tests the dynamic pressure was measured on a micromanometer, one side of which was connected to a "service Pitot tube," while the other side was connected to a static plate in the model test chamber, as shown in Figure 2.

The angle of attack was initially set at 0 degree by the use of a level that was accurate to 1 minute. The angle was varied by means of a calibrated sector on the lift balance.

41630—31——40

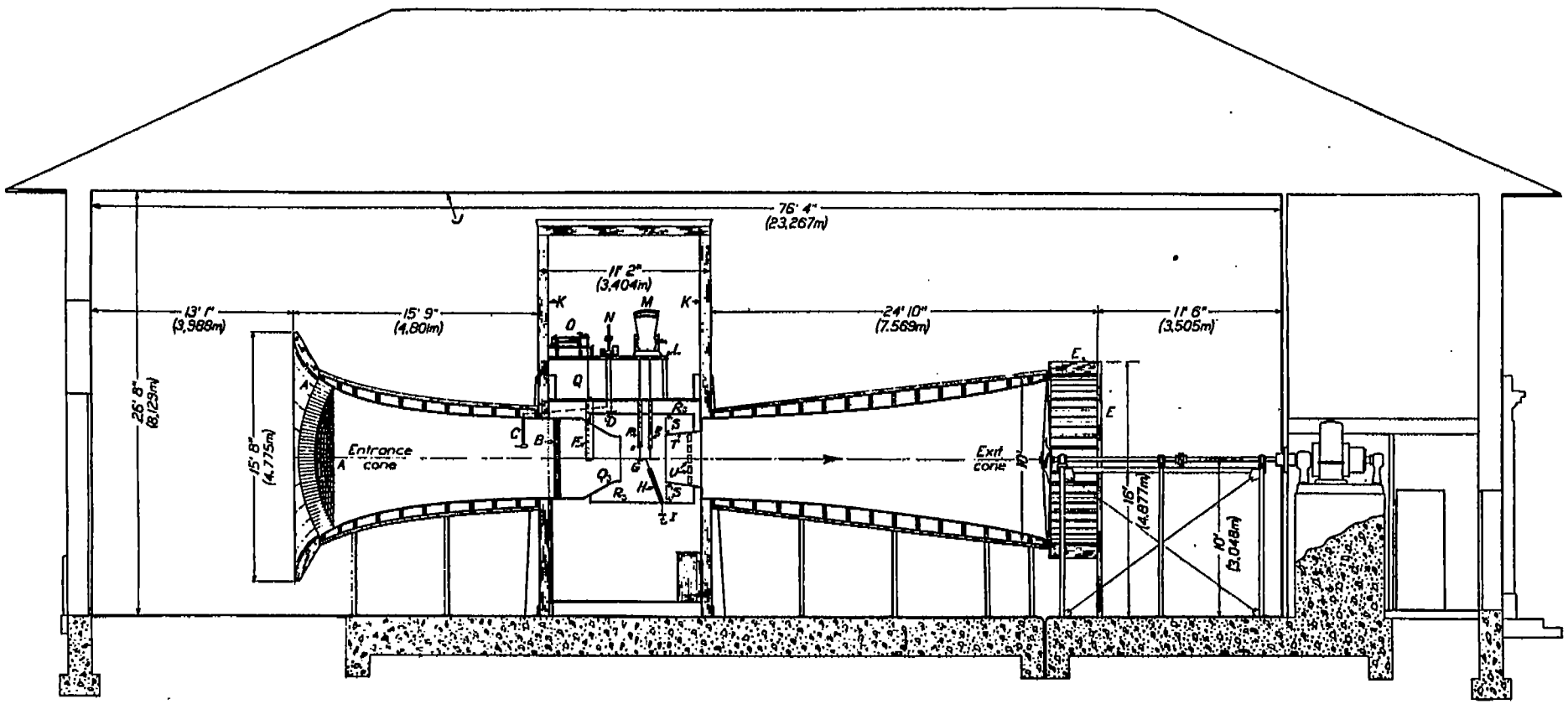

A—Spherical honeycomb (12" × 2½" ± conical tubes), bellmouth of beaver board.
B—Honeycomb-fine (3" × ¾" tubes).
C—Service pitot tube.
D—Static plate in test chamber.
E—Squirrel cage of 48 radial vanes (3' × 9" × ¼") and deflector of beaver board.
F—Streamlined strut for drag wire.
G—Airfoil, inverted.
H—Counterweight wire boot and wire.
I—Counterweight.
J—Ceiling.
K—Experiment chamber wall.
L—Bench for instruments.
M—Lift and moment balance, angle of attack indicator.
N—Micro-manometer.
O—Drag balance.
P—Lift and moment wire boots.
Q—Entrance cone (model).
R—Test chamber (model).
S—Slots in baffle wall.
T—Exit cone (model).
U—Slots in exit cone (model).

FIGURE 2.—N. A. C. A. atmospheric wind tunnel modified for open jet tests

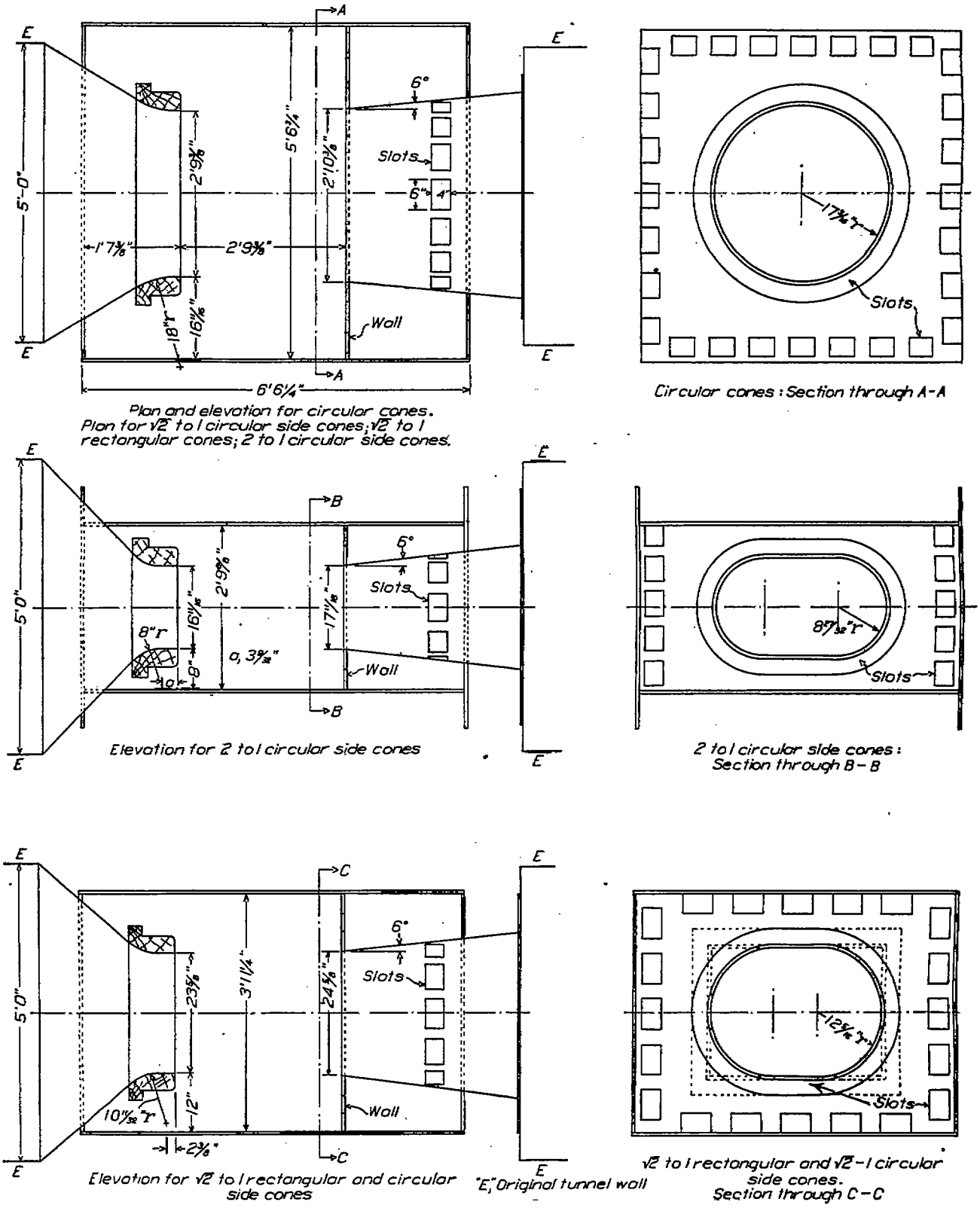

Plan and elevation for circular cones.
Plan for √2 to 1 circular side cones; √2 to 1 rectangular cones; 2 to 1 circular side cones.

Circular cones: Section through A-A

Elevation for 2 to 1 circular side cones

2 to 1 circular side cones: Section through B-B

Elevation for √2 to 1 rectangular and circular side cones

"E," Original tunnel wall

√2 to 1 rectangular and √2-1 circular side cones. Section through C-C

FIGURE 3.—Cone arrangements used in force tests

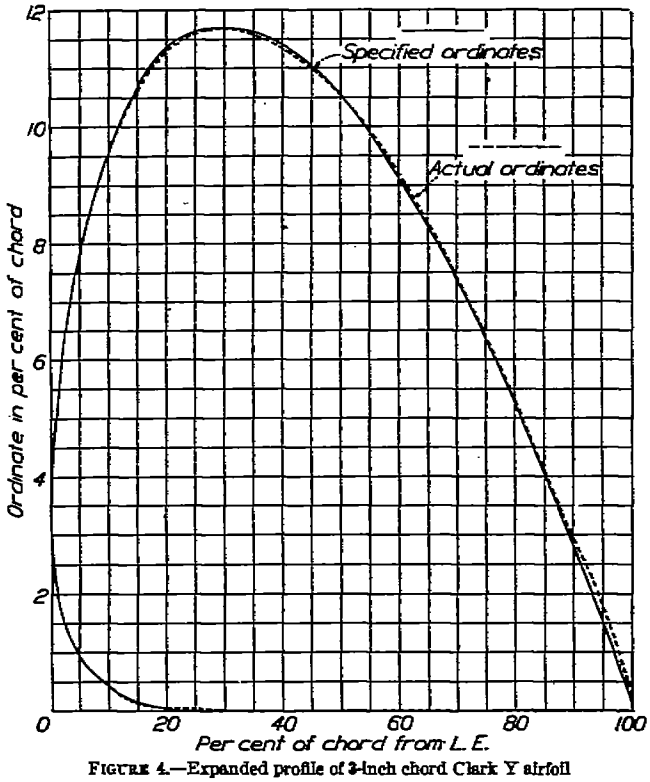

FIGURE 4.—Expanded profile of 3-inch chord Clark Y airfoil

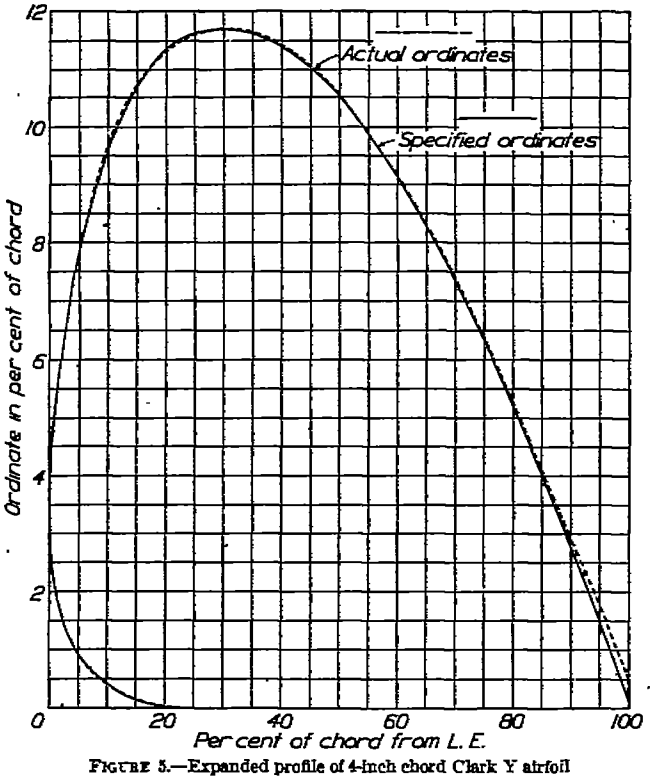

FIGURE 5.—Expanded profile of 4-inch chord Clark Y airfoil

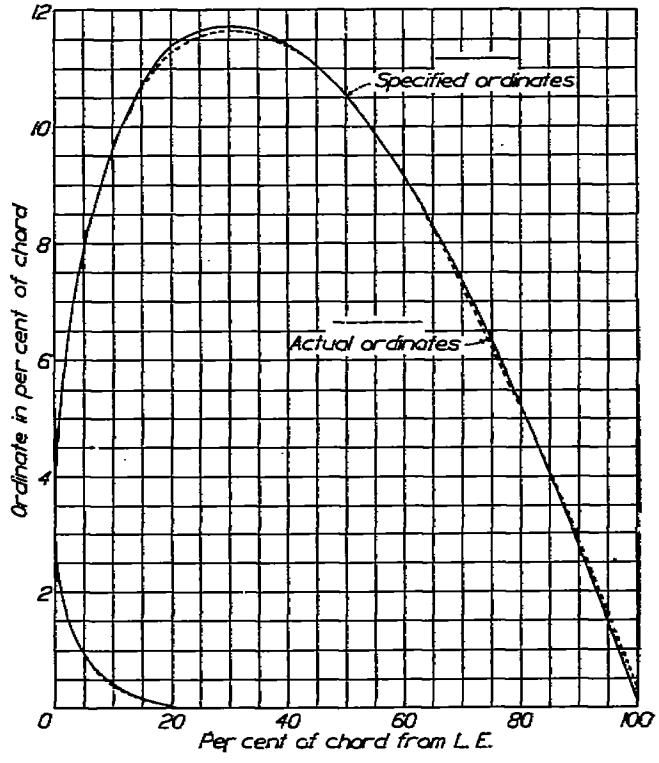

FIGURE 6.—Expanded profile of 5-inch chord Clark Y airfoil

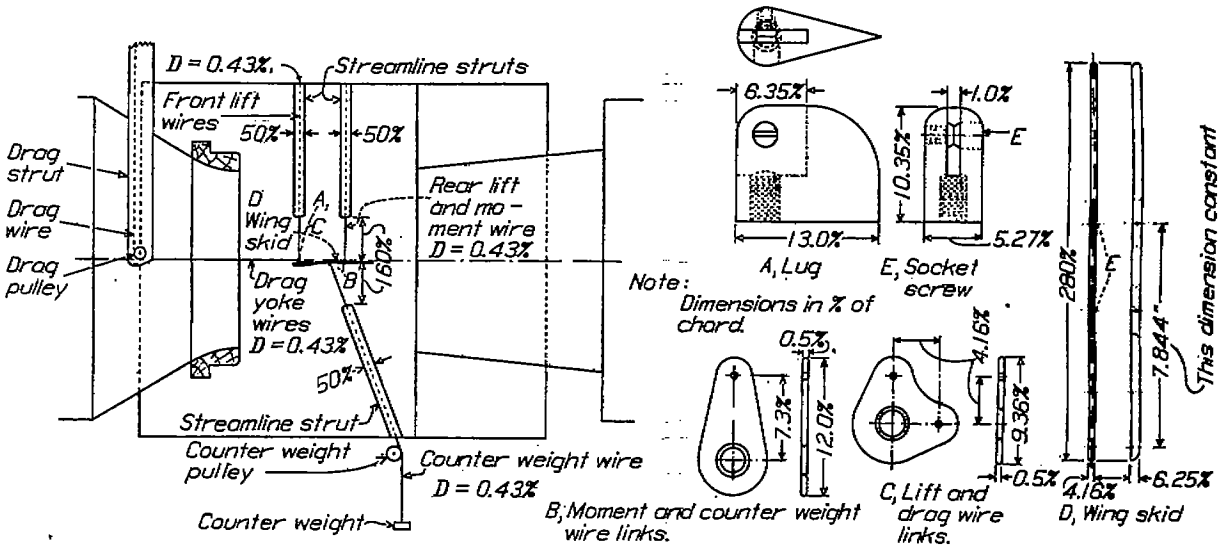

FIGURE 7.—Airfoil set-up in circular jet and details of various fixtures

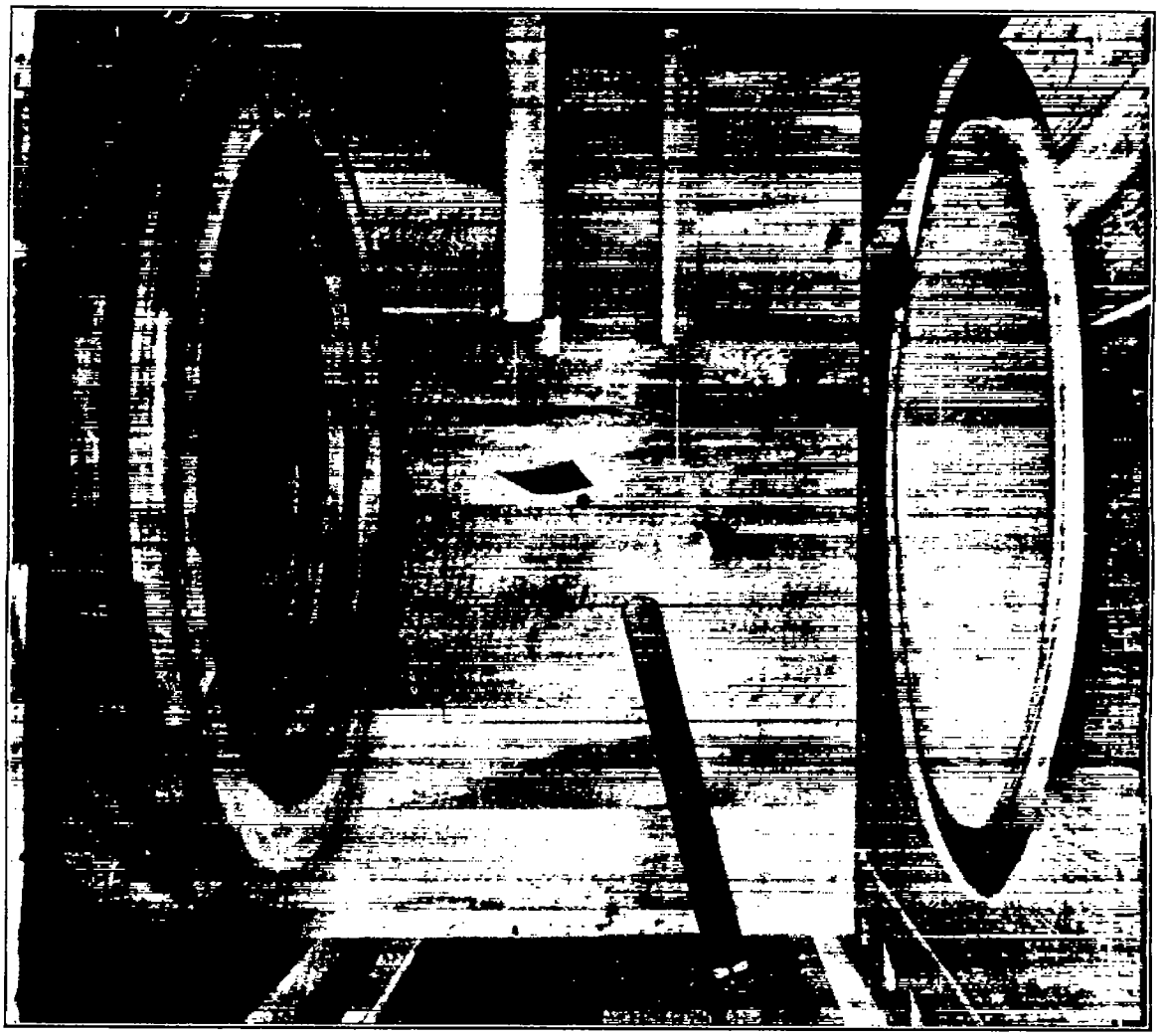

FIGURE 8.—Circular jet with 5-inch chord airfoil set-up

FIGURE 9.—$\sqrt{2}$ to 1 rectangular jet with 5-inch chord airfoil set-up

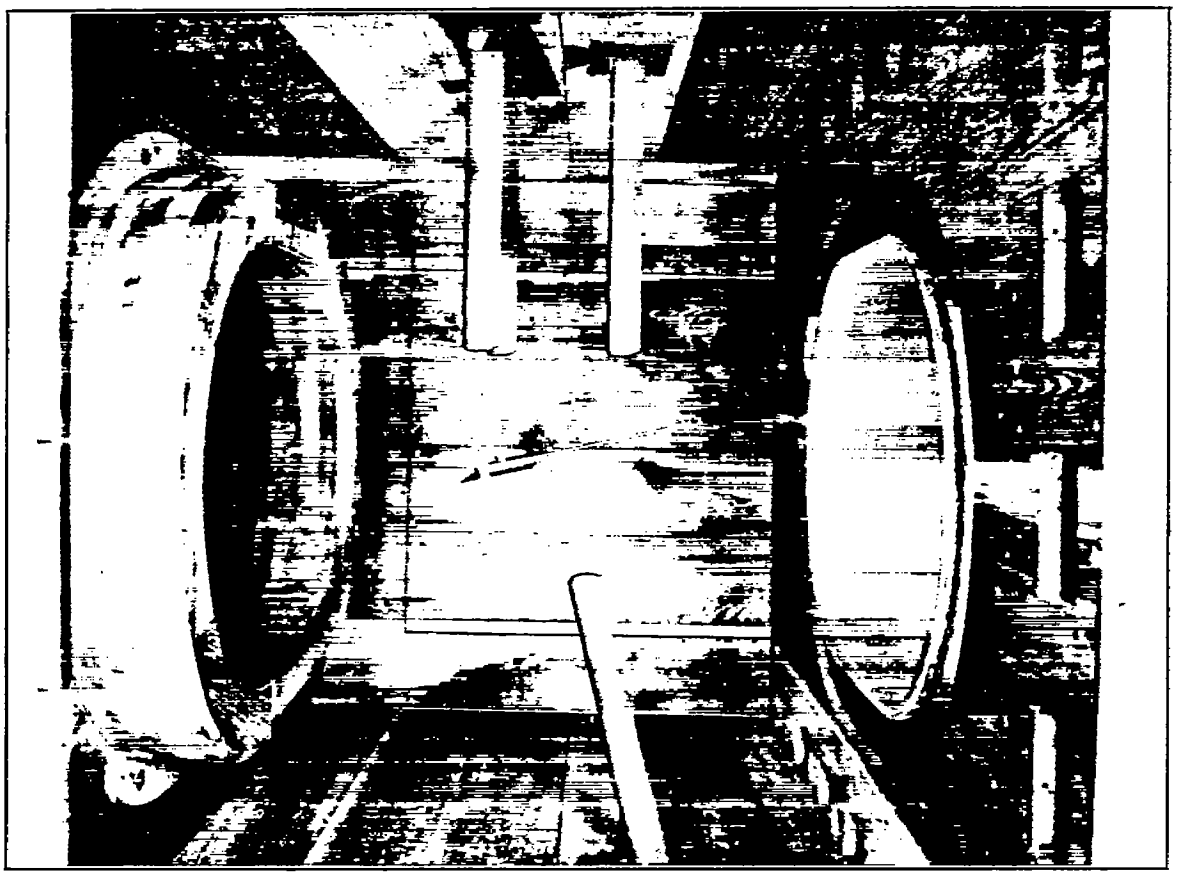

FIGURE 10.—$\sqrt{2}$ to 1 circular side jet with 5-inch chord airfoil set-up

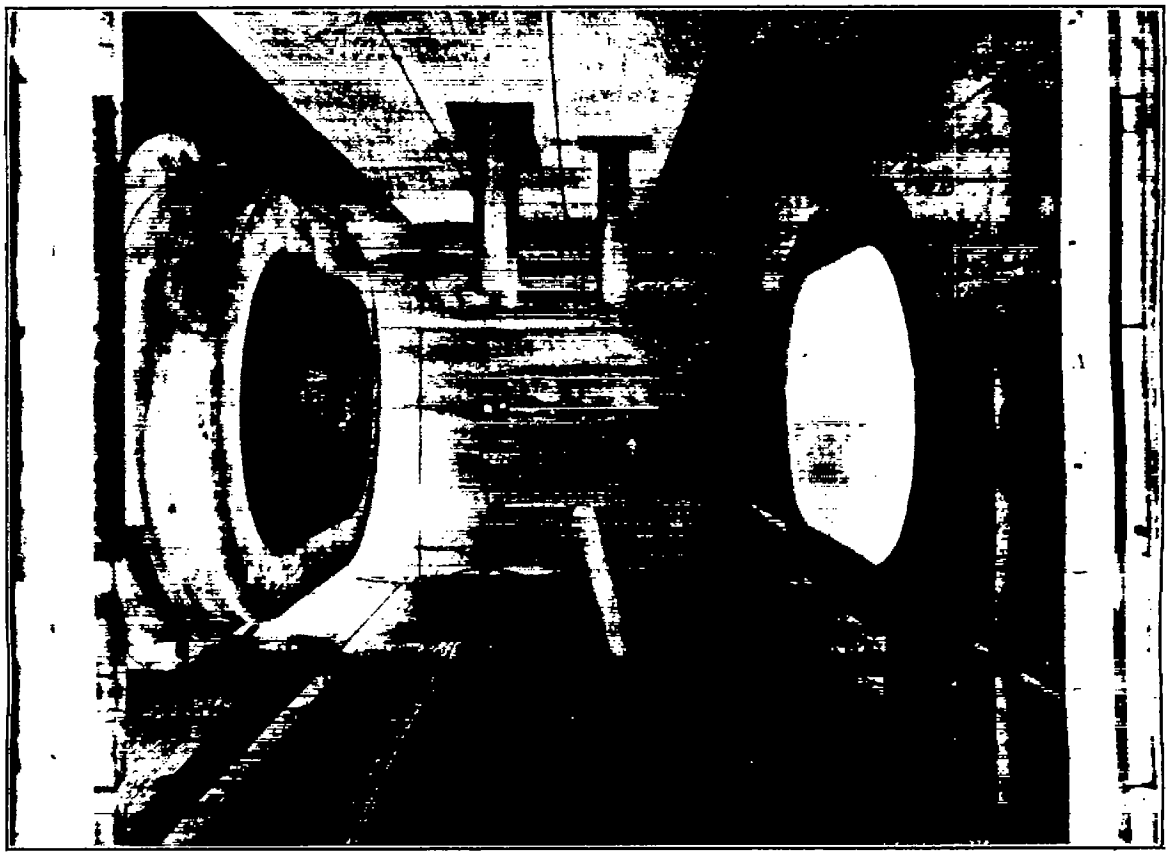

FIGURE 11.—2 to 1 circular side jet with 5-inch chord airfoil set-up

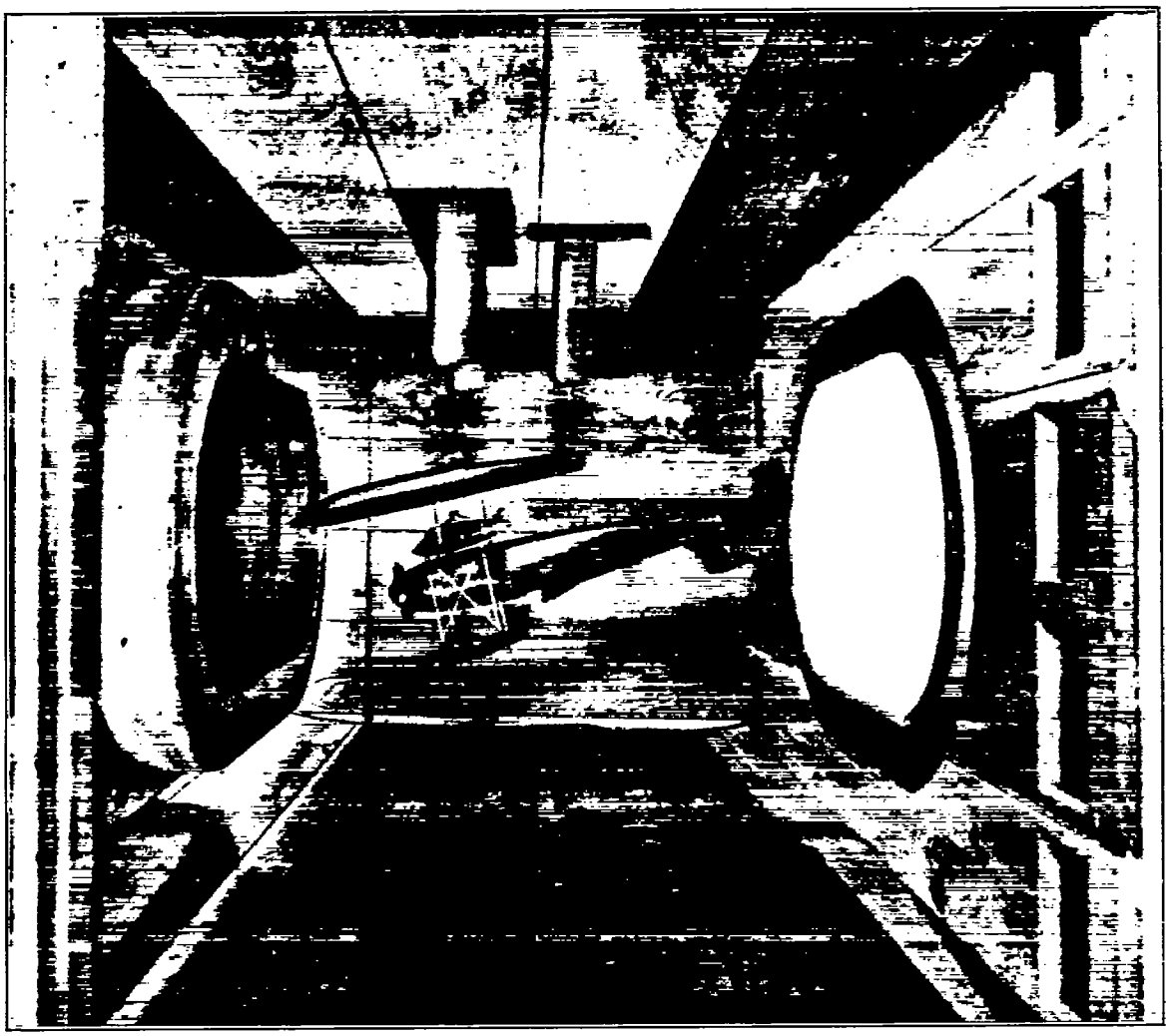

FIGURE 12.—2 to 1 circular side jet with seaplane model set-up

TESTS

Preliminary calibration tests were necessary after the installation of each set of cones. The first test consisted of vertical and horizontal dynamic pressure surveys passing through the centerline of the jet at the location of the quarter-chord point of the models which was about 10 inches downstream from the entrance cone. In addition, a static pressure survey was made in each jet along the centerline from 2 inches ahead of a position corresponding to the quarter chord point of the model position to 18 inches downstream.

All surveys were made at an air speed of about 75 miles per hour, except two additional dynamic pressure surveys in the circular jet at 60 and 100 miles per hour. These additional surveys were made to determine whether different speeds caused any change in the dynamic pressure distribution. This difference was found to be negligible. The service Pitot was next calibrated for several speeds against the integrated mean dynamic pressure at the model position.

Alignment tests were then made in each jet to determine the effective angularity of the air flow with respect to the horizontal. A complete explanation of these tests will be found in the Appendix.

Finally, the airfoils were carefully aligned and tested in each of the four jets. Lift, drag, and pitching moments were measured at 2° intervals over an angle of attack range from zero lift through maximum lift. All tests were made at a Reynolds Number of 225,000, in order to eliminate scale effect. This was accomplished by testing the 3, 4, and 5 inch chord airfoils at velocities of 100, 75, and 60 miles per hour, respectively.

An additional force test was made on the 5-inch chord airfoil, for the purpose of determining roughly the effect of the turbulence produced by a wire screen in the $\sqrt{2}$ to 1 rectangular jet. In this test it was necessary to recalibrate the "service Pitot" on ac-

count of the presence of the screen. This was done by making an additional dynamic pressure survey at the model location. The remaining conditions were the same as in the other airfoil tests.

As previously mentioned, force tests were made on the T. S. seaplane model in each of the four jets to determine the effects of the jet boundaries on the pitching moments. The tail setting was kept constant during these tests. The same range of angles of attack was covered and the same measurements, with the exception of drag, were made as for the airfoil tests. In order to keep the forces on this biplane model within safe limits, it was necessary to make the tests at an air speed of about 40 miles per hour, corresponding to a Reynolds Number of 142,500.

Unusual care was necessary in making the tests in this investigation, since the results depended upon small differences between relatively large quantities. The dynamic pressure was held constant to within ±1 per cent, and the angle of attack was correct to ±0.1°. In order to obtain sufficient accuracy and to prevent erratic results, all the force tests were made in duplicate. The results from the duplicate tests were, in general, within 1 per cent of each other.

RESULTS AND DISCUSSION

Test data:

The dynamic pressure variation at the model location for the various jets is given in Figures 14 to 17. The results of the horizontal and vertical surveys in each jet are plotted in terms of the percentage deviation from the mean value of the dynamic pressure obtained by integration over the region covered by the span of the largest airfoil.

The results from the tests are presented in non-dimensional form in Tables I to XX, and as curves in Figures 18 to 37. The following is a list of symbols used, together with definitions:

$$C_L = \frac{L}{q\,S}$$

$$C_D' = \frac{D'}{q\,S}$$

$$C_M = \frac{M}{q\,C\,S}$$

$$C_p = \left(0.25 - \frac{C_M}{C_L}\right)100$$

$$\alpha_a' = \alpha - \alpha_{L_O}$$

Where: C_L = absolute lift coefficient.

C_D' = absolute drag coefficient with certain preliminary corrections.

C_D = absolute drag coefficient corrected for jet boundary effect.

α_a' = angle of attack in degrees measured from zero lift.

α_a = angle of attack in degrees measured from zero lift and corrected for jet boundary effect.

C_M = absolute moment coefficient with reference to an axis at one-quarter of the chord from the leading edge of the airfoil model. In the seaplane results this coefficient is about the center of gravity.

C_p = center of pressure location from the leading edge of the model.

α = geometrical angle of attack as measured with respect to the chord line.

α_{L_O} = geometrical angle of attack of zero lift.

L = measured lift.

D' = measured drag with preliminary corrections.

M = measured pitching moment.

S = area of airfoil.

c = chord of airfoil.

q = mean dynamic pressure over span of model.

Preliminary corrections.

Certain preliminary corrections to the test data were necessary before the correction factors for jet

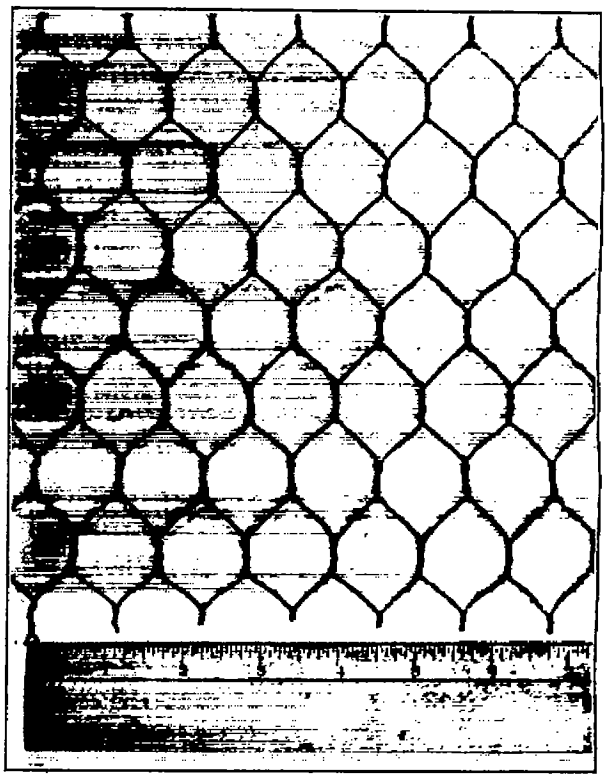

FIGURE 13.—Wire mesh used in turbulence tests

boundary effect could be calculated. First, the actual angle of attack was slightly larger than the measured angle due to the stretch in the lift wires. To correct for this the elongation of the wires was calculated. This correction amounted to a maximum of about 0.3°, which occurred in the case of the smallest airfoil set-up. After applying this correction, the curves of lift versus angle of attack still showed variations at

zero lift. This difference may have been partly due to slight differences in profile, as shown in Figures 4 to 6, and also to inaccuracies in the initial setting of the

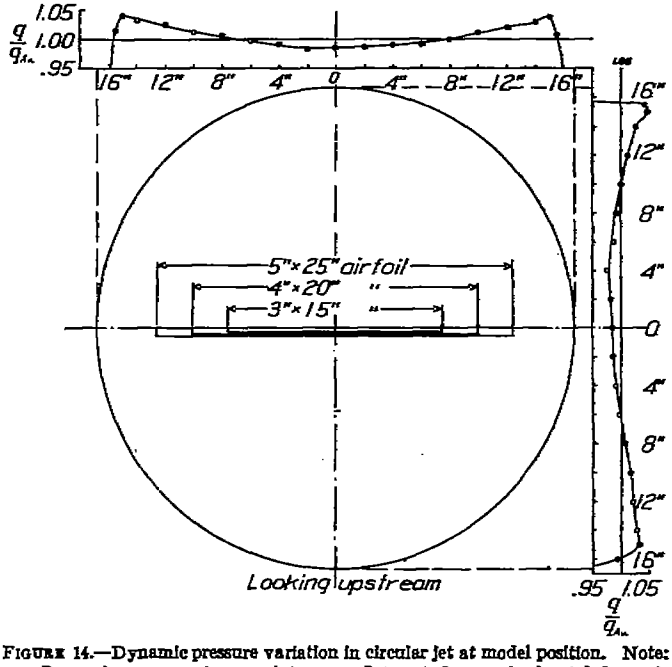

FIGURE 14.—Dynamic pressure variation in circular jet at model position. Note: q=Dynamic pressure at any point. q_{AV}=Integrated mean horizontal dynamic pressure over span of 5-inch by 25-inch airfoil

wing. The measured angle of zero lift was subtracted from each angle of attack to eliminate this difference.

Preliminary corrections for drag were also made. These corrections were necessitated by buoyancy due

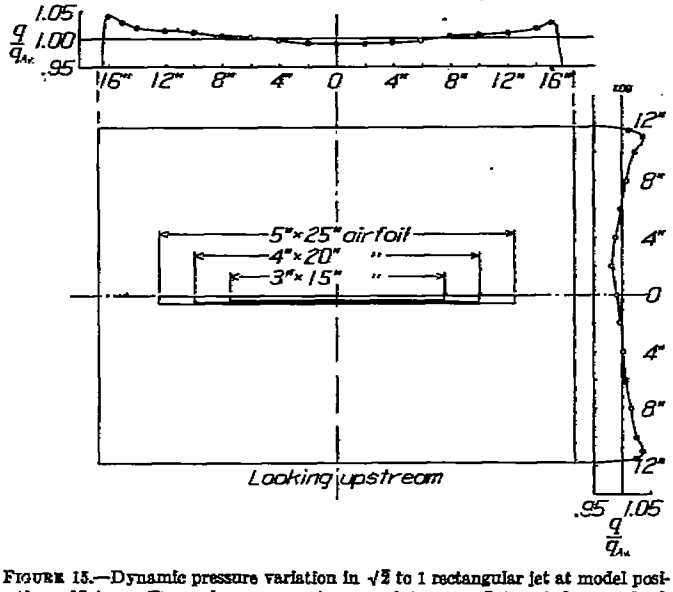

FIGURE 15.—Dynamic pressure variation in $\sqrt{2}$ to 1 rectangular jet at model position. Note: q=Dynamic pressure at any point. q_{AV}=Integrated mean horizontal dynamic pressure over span of 5-inch by 25-inch airfoil

to the relatively large longitudinal static pressure gradient in the jets, by small differences in the profiles of the three airfoils, and by the effects of turbulence.

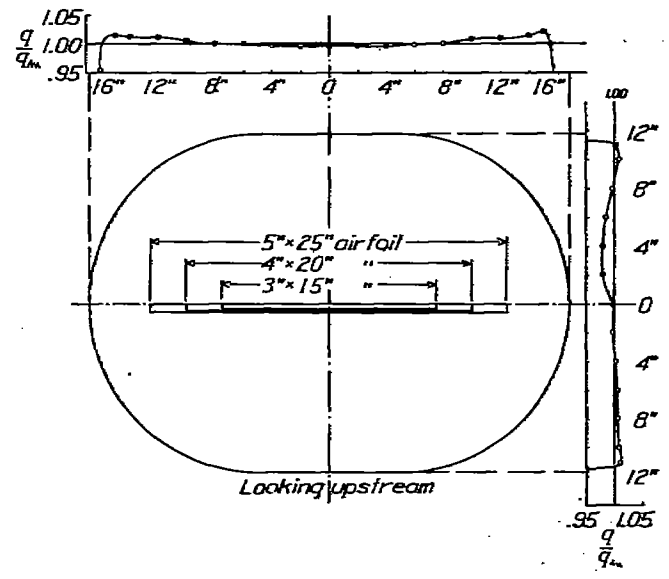

FIGURE 16.—Dynamic pressure variation in $\sqrt{2}$ to 1 circular side jet at model position. Note: q=Dynamic pressure at any point. q_{AV}=Integrated mean horizontal dynamic pressure over span of 5-inch by 25-inch airfoil

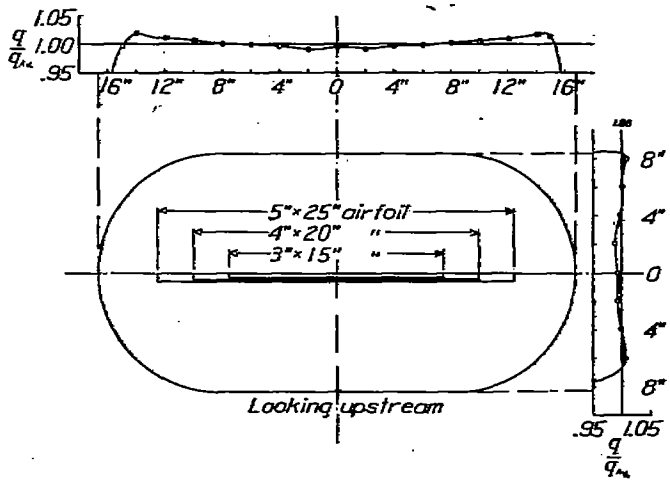

FIGURE 17.—Dynamic pressure variation in 2 to 1 circular side jet at model position. Note: q=Dynamic pressure at any point. q_{AV}=Integrated mean horizontal dynamic pressure over span of 5-inch by 25-inch airfoil

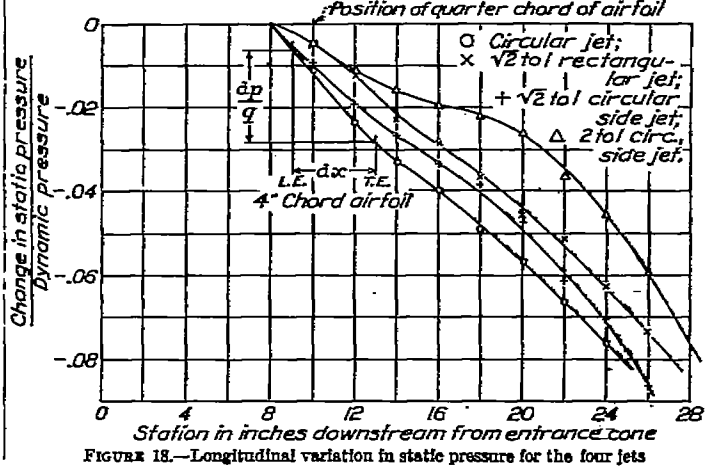

FIGURE 18.—Longitudinal variation in static pressure for the four jets

The effect of longitudinal static pressure variation on the drag of an airfoil is usually neglected. In these tests, however, it was found that the static pressure gradient caused differences of as much as 10 per cent in minimum measured drag. Figure 18 shows the longitudinal static pressure characteristics of each of the four jets. The method of correcting the drag for this effect is given in Reference 9, and is as follows:

$$x = A' \frac{dp}{dx} \tag{1}$$

where x = drag due to static pressure variation,

A' = effective volume of model,

$\frac{dp}{dx}$ = static pressure gradient at any point along the jet centerline.

Equation (1) may be reduced to the following coefficient form:

$$C_x = \frac{A'}{q\,S}\frac{dp}{dx}.$$

The term $\frac{1}{q}\frac{dp}{dx}$ was obtained as shown in Figure 18. The effective volume A' for an airfoil was taken as 1.1 times the actual volume. (See Reference 9.) This drag coefficient increment, C_x, varied with the different jets and airfoils, but was considered practically constant at a l angles of attack for a given airfoil jet combination. This is not strictly true, but since the percentage correction is appreciable only at small values of drag, the errors introduced by this assumption are negligible. Since the static pressure decreased in the downstream direction, C_x was subtracted from the drag coefficient.

After this correction had been applied it was found that there was still a considerable variation in minimum drag. Since at the angle of attack of minimum drag the induced drag was negligible, the variation in the measured drag was due to other than jet boundary effects. It will be noted that since the various entrance cones were all fitted to the same part of the original tunnel throat, the ratio of the areas of the large end to the small end of each cone was different. That this difference probably had an effect on drag is shown in Figure 19–A, in which curves of minimum drag coefficient are plotted versus area reduction in the different entrance cones. The individual curves show that for the three airfoils in the same jet there is a consistent difference which may be attributed to inaccuracies in the profiles. (See Figures 4, 5, and 6.)

The mean values are also plotted in the figure and show that for all the airfoils there is a decrease in drag coefficient with an increase in entrance cone reduction. The only reasonable explanation that seems to be left is that this variation was due to differences in turbulence in the different jets, and it may be assumed that the turbulence decreased with increasing area reduction (Reference 10). In addition, the recent work of Dryden on turbulence (Reference 3) shows that increasing the turbulence results in an increase in the drag coefficient of airships, and he predicts increased drag also for airfoils under these conditions. In order to check this prediction, an additional force test was made in the rectangular jet with wire mesh (fig. 13) stretched across the entrance cone, as mentioned above. The results of the tests on the same airfoil with and without the screen are given in Figure 20 and Table I, and show that the profile drag, C_{D_0}, increases with turbulence at small lift coefficients as predicted. Thus, turbulence may be considered to account for the discrepancy between the mean drag coefficients in the different cones. It will be noted in Figure 19–A that the average curve of minimum C_D becomes asymtotic at the larger values of area reduction which represents small degrees of jet turbulence.

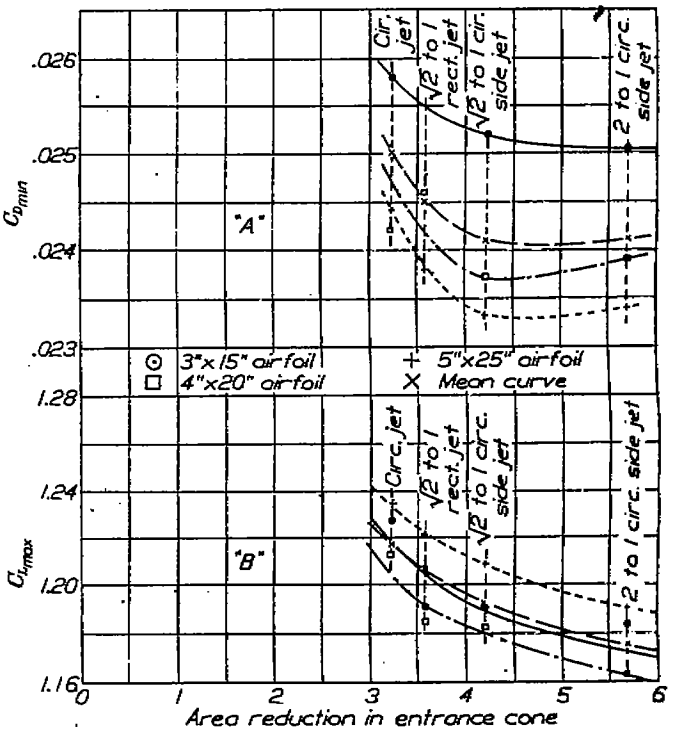

FIGURE 19.—Variations in minimum drag and maximum lift for all tests

Thus, it appears that $C_{D_{min.}} = 0.0241$ may be considered to represent practically nonturbulent flow, at least in so far as small values of drag for the airfoil set-ups are concerned.

The observed drag corrected for static pressure gradient was now corrected for the effects of profile inaccuracy and turbulence by adding or subtracting a factor which was assumed to be independent of angle of attack, but which varied with each test, as shown in Figure 19–A. This merely means that the drag coefficient curves were adjusted so that all had the same minimum value, $C_{D_{min.}} = 0.0241$. Thus, the data when finally corrected for jet boundary effect may be considered to represent free air conditions without turbulence.

Maximum lift is also affected by profile inaccuracies and turbulence as shown in Figures 19–B and 20. However, no corrections were derived for these dis-

crepancies because of the critical nature of the flow at the large angles of attack.

The differences in the dynamic pressure distribution in the various jets, Figures 14 to 17, caused negligible differences in the force test results. This was due to the fact that in each force test the dynamic pressure was taken as the mean value obtained by integration of the survey from tip to tip of the particular airfoil.

Jet boundary corrections.

After the preliminary corrections had been applied, the data were in the proper form for the determination of the jet boundary corrections. The first step taken was the calculation of the corrections for the three airfoils in the circular jet by the theoretical method derived by Prandtl, as given in Reference 6. The method is based on the assumption of elliptical lift distribution over the airfoil span, and the equations are as follows:

$$\Delta\alpha_i = \delta \frac{S}{A} C_L \tag{4}$$

and

$$\Delta C_{D_i} = \delta \frac{S}{A} C_L^2 \tag{5}$$

where

$$\delta = \frac{1}{8}\left(1 + \frac{3}{16}\left(\frac{b}{D}\right)^4 + \cdots\right) \tag{6}$$

$\Delta\alpha_i$ = angle of attack induced by jet boundaries.
ΔC_{D_i} = coefficient of drag induced by jet boundaries.
C_L = lift coefficient.
S = area of airfoil.
D = diameter of the jet.
b = span of airfoil.
A = cross-sectional area of the jet.

For open jets the corrections $\Delta\alpha_i$ and ΔC_{D_i} are to be subtracted from α and C_D', respectively.

It will be seen that two factors enter into these corrections, i. e., $\frac{S}{A}$ and $\left(\frac{b}{D}\right)^4$. Of these the ratio of the areas, $\frac{S}{A}$, is by far the more important, but when the ratio of span to jet diameter exceeds $\frac{3}{4}$, the $\frac{b}{D}$ term becomes appreciable.

For convenience in the following analysis, Equations (4) and (5) may be written:

$$\delta_\alpha = \frac{\Delta\alpha_i}{C_L \frac{S}{A} \frac{180}{\pi}} \tag{7}$$

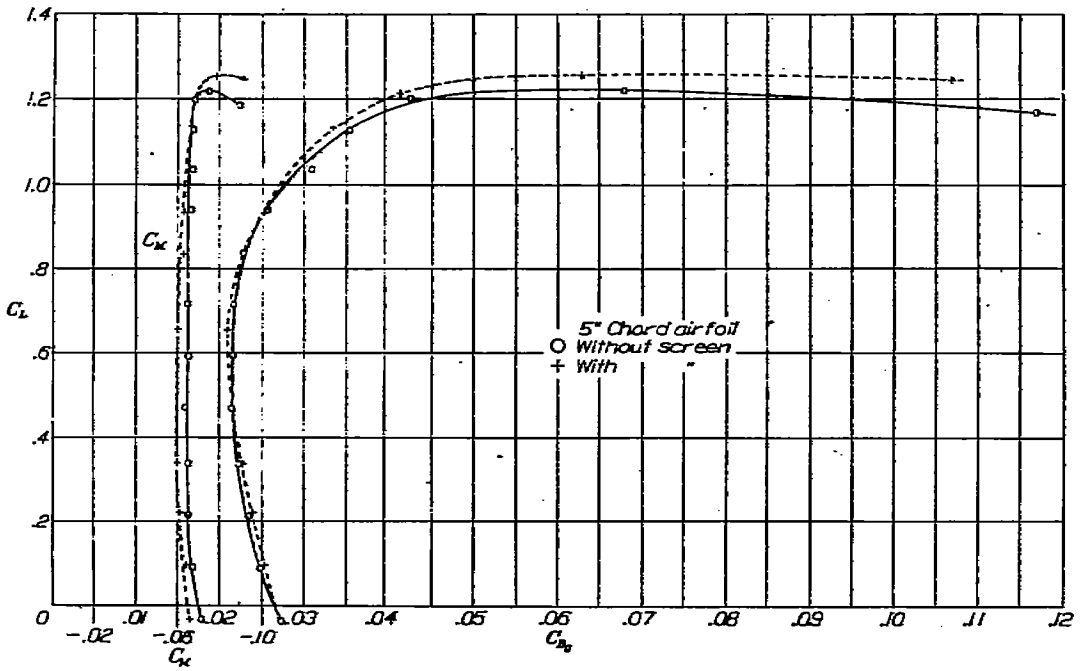

FIGURE 20.—Lift and moment versus profile drag showing effect of turbulence in the $\sqrt{2}$ to 1 rectangular jet

and

$$\delta_D = \frac{\Delta C_{D_i}}{C_L^2 \frac{S}{A}} \tag{8}$$

where $\Delta\alpha_i$ is now expressed in degrees,
δ_α = correction factor for angle of attack.
δ_D = correction factor for drag.

The values of δ_α and δ_D were next determined from the experimental data. This was done in the case of δ_α by extrapolating to free air conditions $\left(\frac{S}{A}=0\right)$ the curves drawn through the values of angle of attack for the same lift on each airfoil (see fig. 21). The difference between the intercept at $\frac{S}{A}=0$ and the measured angle of attack of a particular airfoil was $\Delta\alpha_i$, which, when used in Equation (6), together with suitable values of C_L and $\frac{S}{A}$, gave δ_α. The final value

of δ_α was the average obtained from the extrapolation of the curves for 11 different values of lift as shown in Figure 21. The same procedure was used in obtaining δ_D from Equation (7), drag instead of angle of attack being the dependent variable, as shown in

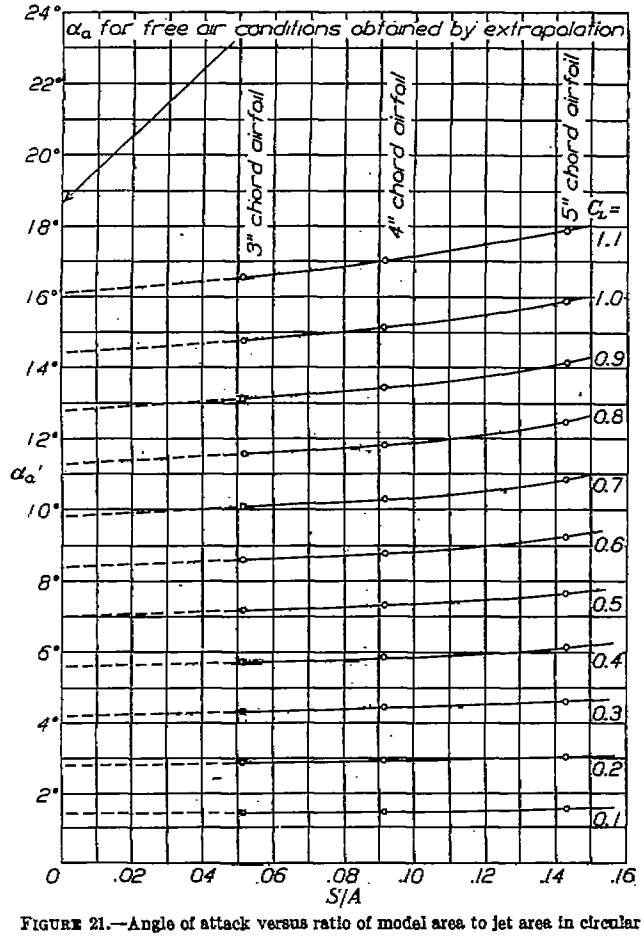

FIGURE 21.—Angle of attack versus ratio of model area to jet area in circular jet for determining δ_α

Figure 22. The data for obtaining these two correction factors are given in Tables II and III.

A comparison of the theoretical and experimental values of δ_α and δ_D for the three airfoils in the circular jet may be made by reference to Figure 23 and Table IV. The agreement between the 3 and 4 inch chord airfoil results is excellent, but for the 5-inch chord airfoil the experimental values are greater than the theoretical, and δ_α is considerably larger than δ_D. This indicates that the lift distribution over the span of this airfoil has been modified by the jet boundaries so that it is no longer approximately elliptical.

It was assumed, by reason of the agreement of the theoretical and experimental correction factors for the 3 and 4 inch chord airfoils, that the corrected angles of attack and drag represented free air conditions for these models. The correction factors for the other jets were determined on the basis of this assumption.

These remaining values of δ_α and δ_D were obtained from Equations (6) and (7) by substituting the proper values of $\Delta\alpha_i$ and ΔC_{D_i}, respectively, for a given value of C_L. These angle of attack and drag increments are as follows:

$$\Delta\alpha_i = \alpha_a' - \alpha_a$$

and

$$\Delta C_{D_i} = C_D' - C_D$$

where α_a' and C_D' are the angle of attack and drag coefficient, respectively, as determined from the tests with preliminary corrections applied, and where α_a and C_D are the angle of attack and drag coefficient, respectively, for free air conditions as determined from the extrapolated curves (figs. 21 and 22) and from the theoretical corrections. The final values of δ_α and δ_D are, as before, the average of the values obtained for several different lift coefficients.

The correction factors for all four jets are plotted in Figures 23 to 26 against the ratio of model span to

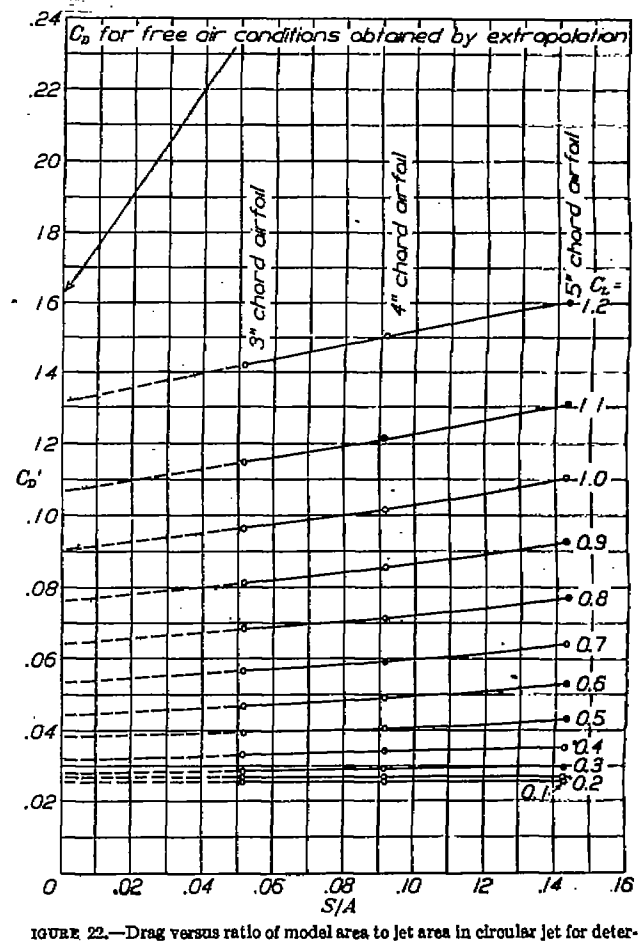

IGURE 22.—Drag versus ratio of model area to jet area in circular jet for determining δ_α

width of jet. It will be seen that large differences exist between the factors both for the various jet shapes and also for the different airfoils. Moreover, except for the 4-inch chord airfoil in the rectangular

jet, δ_α is greater than δ_D. It is believed that all these discrepancies may be attributed to the departure from the assumed elliptical distribution of lift, and doubtless represent a change in the series of Equation (6). As might be anticipated on this basis, the correction factors show an increase as the jet depth is decreased. The effect of the semicircular sides on the $\sqrt{2}$ to 1

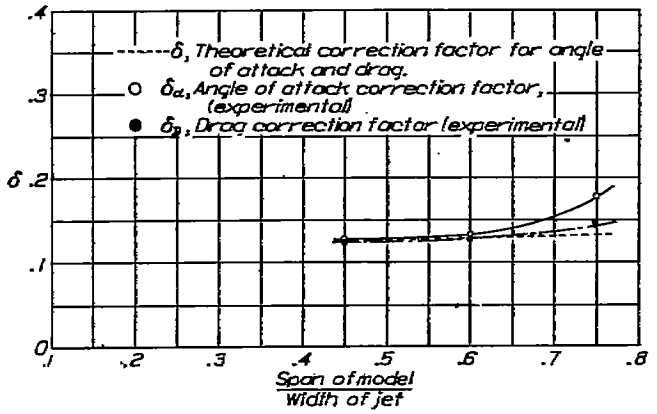

FIGURE 23.—Correction factors versus ratio of model span to jet width for circular jet

jet is to decrease somewhat the magnitude of the factors as compared with those for the rectangular jet.

The validity of these corrections for angle of attack and drag as given by Equations (4) and (5) was then tested by using them to correct all the wind tunnel results to free air conditions. Figures 27 to 34 are curves of lift and drag versus angle of attack and the polar for each airfoil in the four jets, together with the corresponding free air curves for comparison. The data from

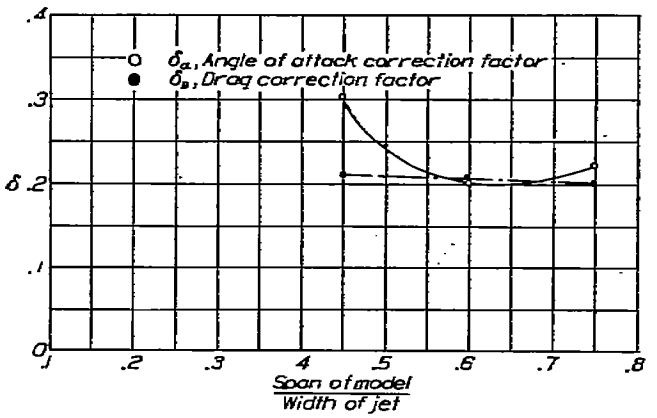

FIGURE 24.—Correction factors versus ratio of model span to jet width for $\sqrt{2}$ to 1 rectangular jet

which these figures were obtained are given in Tables V to XVI. These curves to which the preliminary corrections have been applied show the magnitude of the discrepancies due to the jet boundaries. The final corrected results for all the tests are plotted together in Figures 35 and 36. Each curve contains 168 points representing 336 individual measurements. It will be seen that the corrections are quite satisfactory up as far as the angle of maximum lift, beyond which, as might be expected, the points scatter considerably. This scattering is probably due to profile inaccuracies and to turbulence in the jet, both of which produce relatively large changes in flow in this region. This is shown in greater detail in Figures 19–B and 20, as mentioned above.

It has been hitherto demonstrated both theoretically and experimentally that the pitching moment and

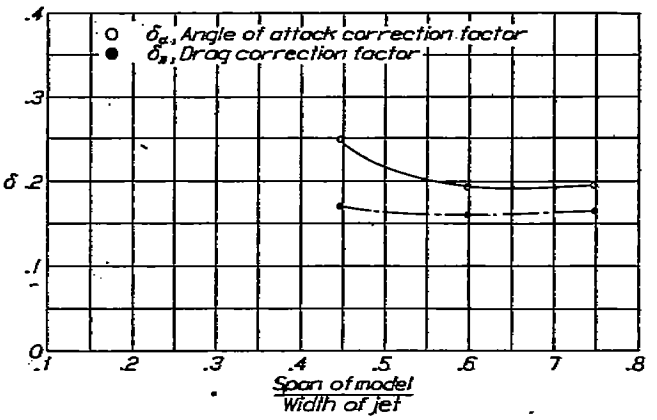

FIGURE 25.—Correction factors versus ratio of model span to jet width for $\sqrt{2}$ to 1 circular side jet

center of pressure remain the same for any airfoil in either two or three dimensional flow (Reference 11). In other words, these two characteristics are independent of the lift distribution. The center of pressure curve is given in Figure 35 and the curve of moment coefficient about the quarter-chord point, in Figure 36. No corrections were applied except for the center of pressure which was plotted on the same angle of attack basis as C_L and C_D. The agreement is satis-

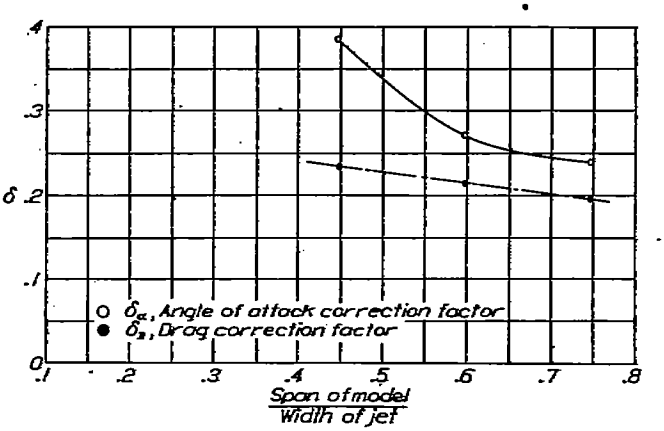

FIGURE 26.—Correction factors versus ratio of model span to width of jet for 2 to 1 circular side jet

factory, and such discrepancies as exist may be attributed also to profile inaccuracies and to differences in turbulence. The latter explanation is based on the difference between the two moment curves obtained from the turbulence tests as given in Figure 20.

The results of the pitching moment tests on the seaplane model are given in Tables XVII to XX and in Figure 37, where pitching moment coefficient, C_M, about the *C. G.* is plotted against C_L for the four tests. The agreement may be considered satis-

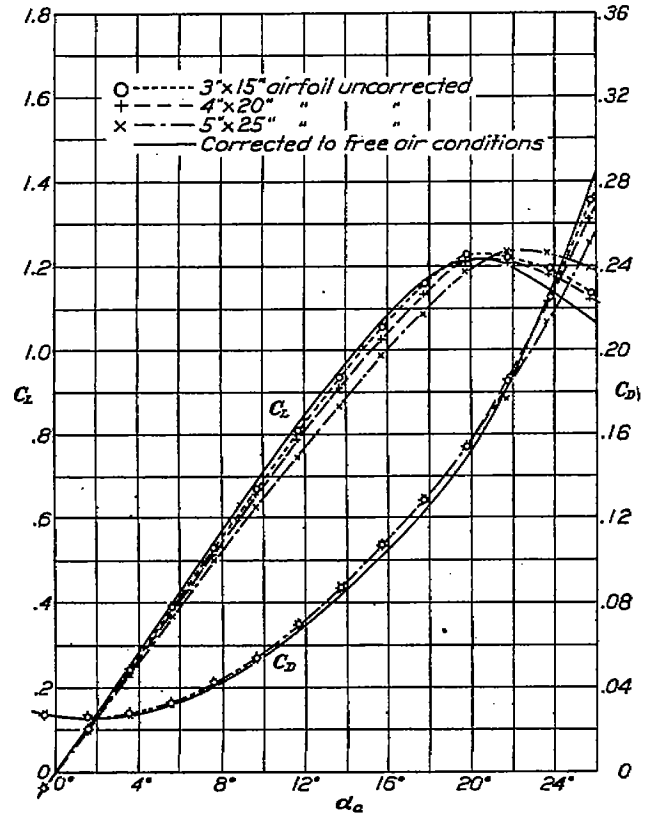

FIGURE 27.—Lift and drag versus angle of attack for three airfoils in circular jet

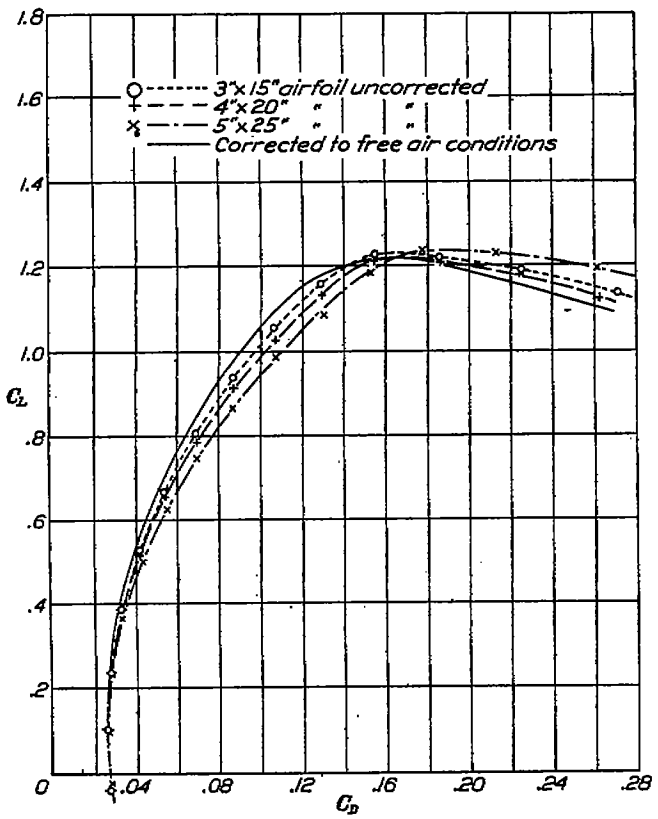

FIGURE 28.—Lift versus drag for three airfoils in the circular jet

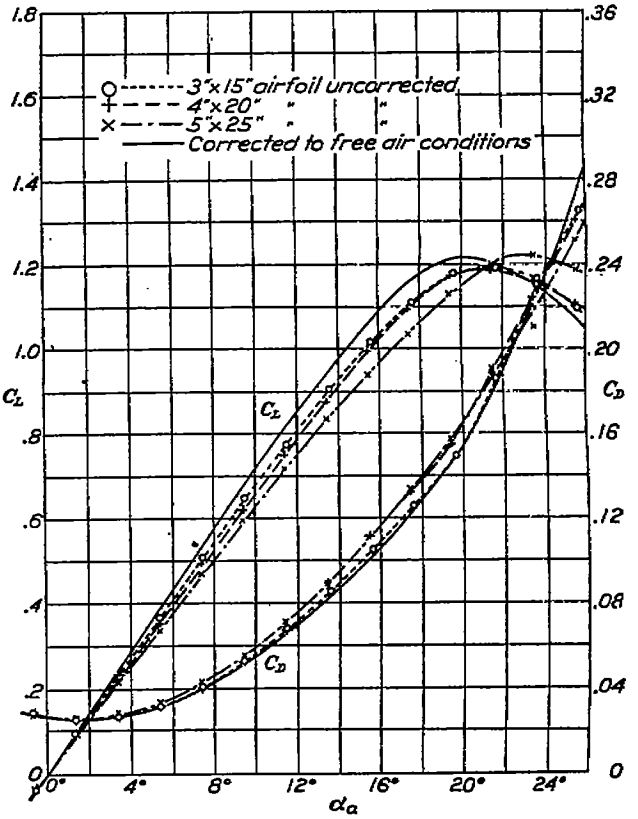

FIGURE 29.—Lift and drag versus angle of attack for three airfoils in $\sqrt{2}$ to 1 rectangular jet

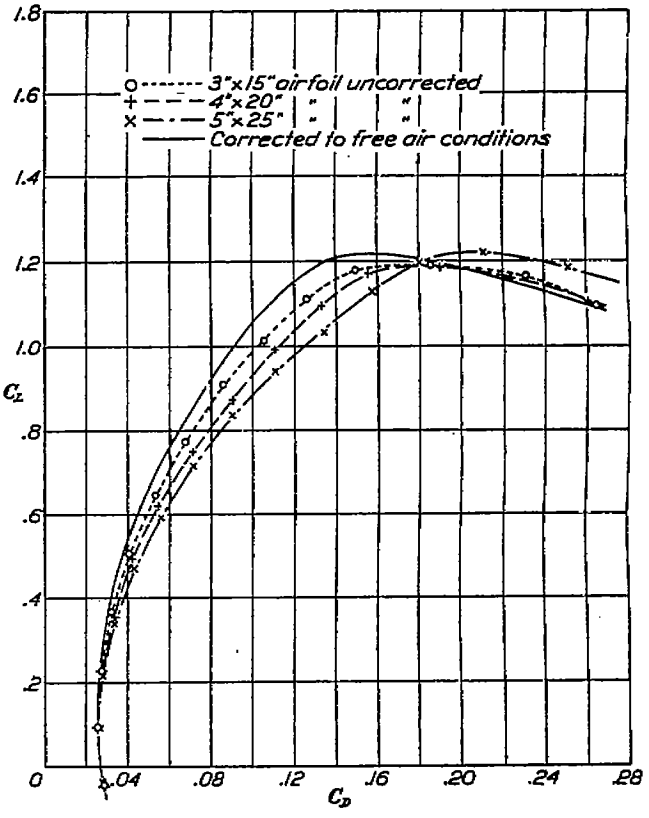

FIGURE 30.—Lift versus drag for three airfoils in $\sqrt{2}$ to 1 rectangular jet

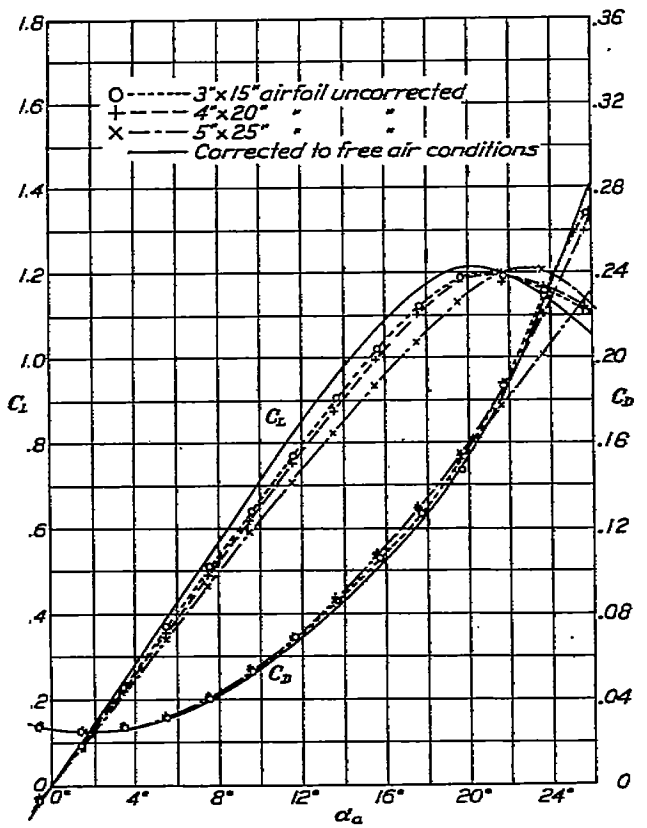

FIGURE 31.—Lift and drag versus angle of attack for three airfoils in $\sqrt{2}$ to 1 circular side jet

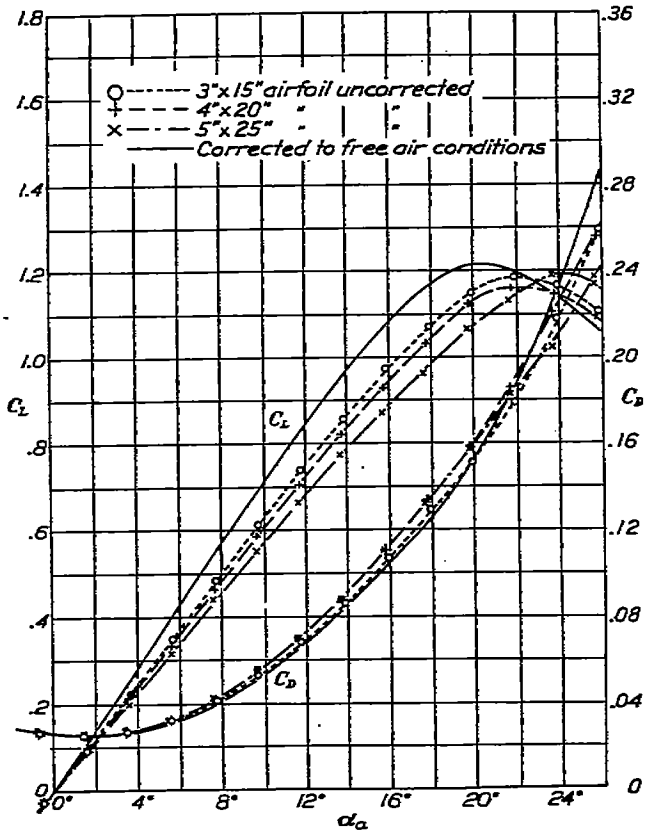

FIGURE 33.—Lift and drag versus angle of attack for three airfoils in 2 to 1 circular side jet

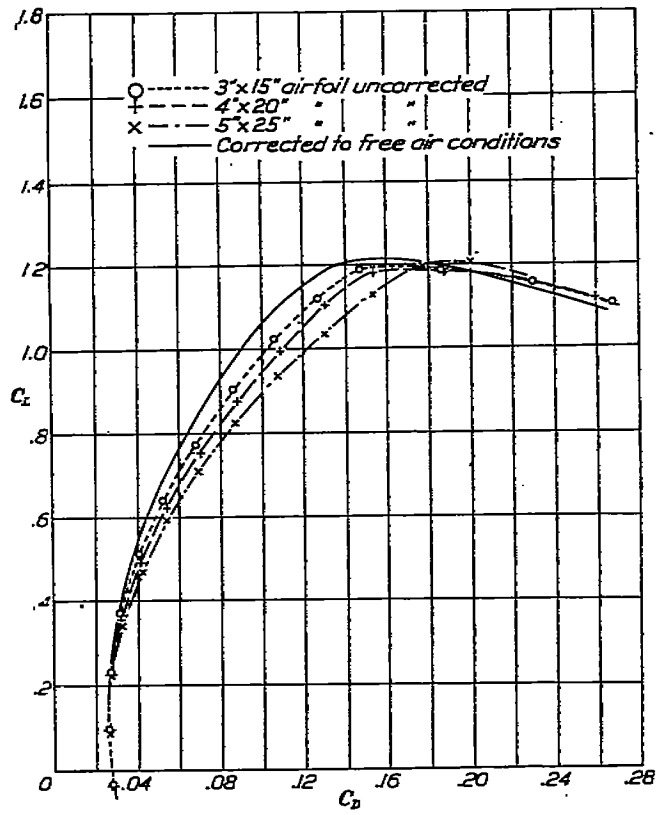

FIGURE 32.—Lift versus drag for three airfoils in $\sqrt{2}$ to 1 circular side jet

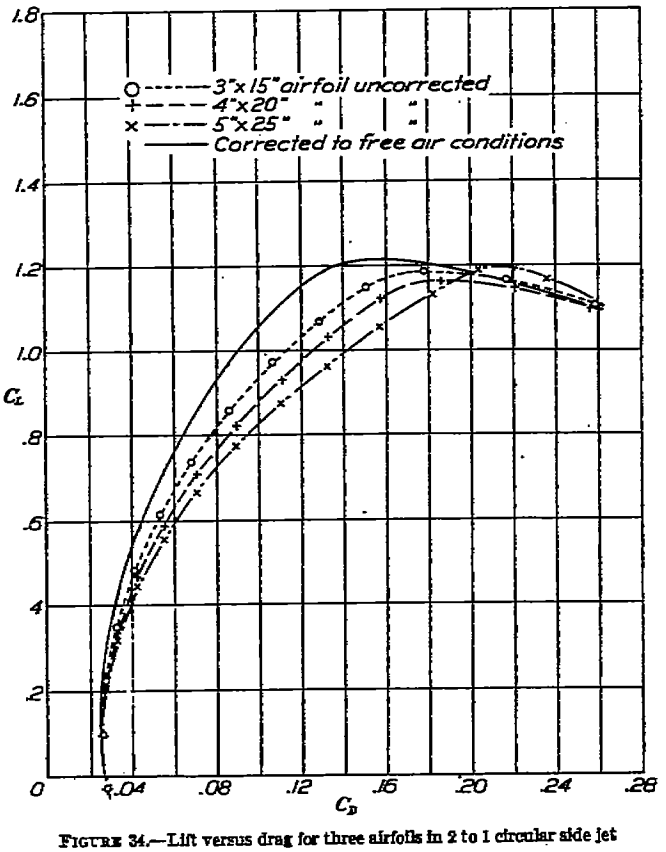

FIGURE 34.—Lift versus drag for three airfoils in 2 to 1 circular side jet

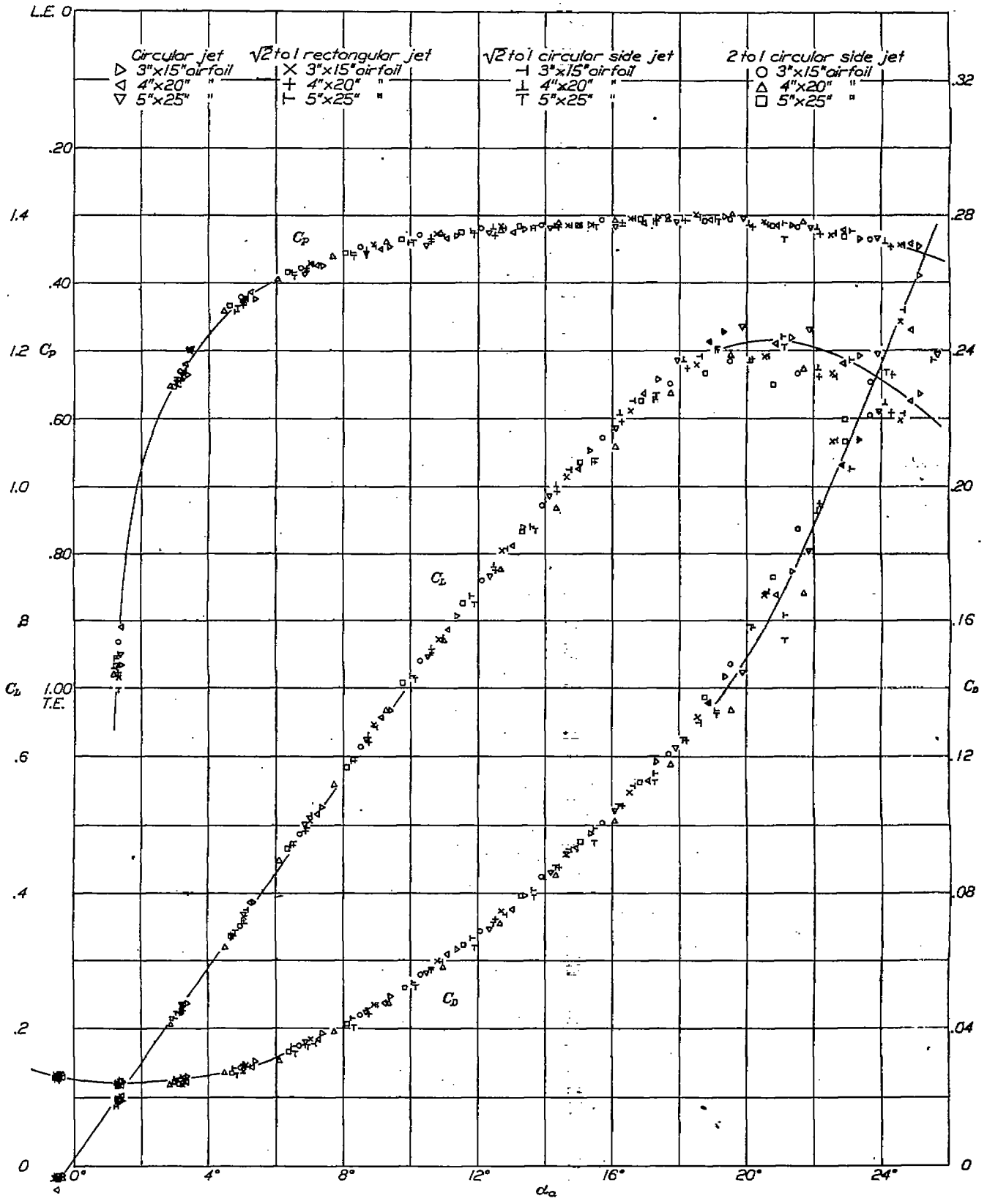

FIGURE 35.—Lift, drag, center of pressure versus angle of attack for three airfoils in four jets corrected to free air conditions

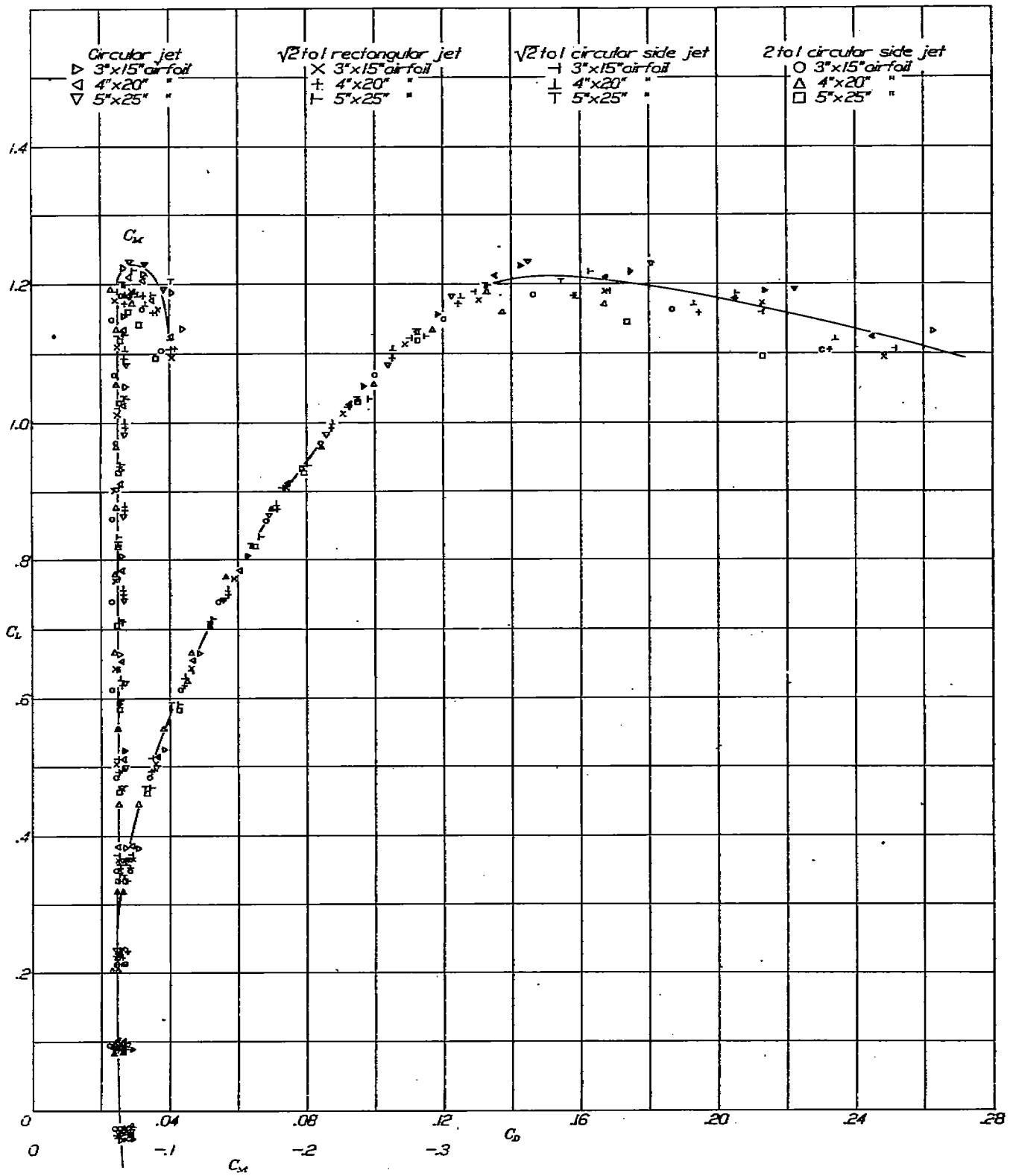

FIGURE 38.—Lift versus drag and pitching moment for three airfoils in four jets corrected to free air conditions

factory with the exception of the tests in the 2 to 1 circular side jet. In these tests the upper wing of the model was apparently too near the bottom of the jet, as shown in Figure 12, and hence was probably in a region of low velocity. As the angle of attack was increased the wing was raised into a region of higher velocity, which would account for the better agreement in the moments at values of C_L greater than 0.8.

It is evident that the change in lift distribution produced by the jet boundaries did not appreciably modify the downwash, and consequently the pitching moment due to fuselage and horizontal tail at a given lift coefficient, was independent of the shape of the jet.

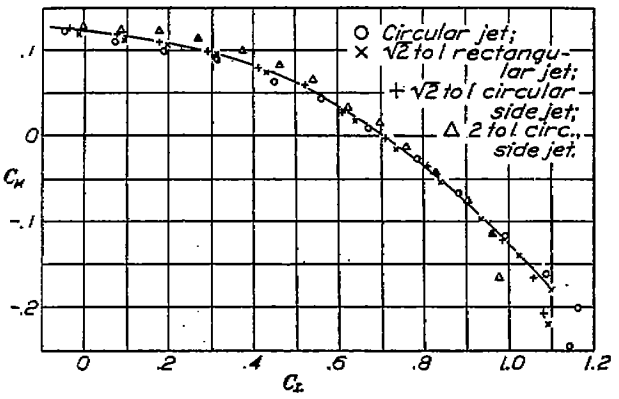

FIGURE 37.—Pitching moment versus lift for T. S. seaplane model in four jets

However, if it were desired to plot C_M against α, it would be necessary to correct for the angle of attack increment, $\Delta\alpha_t$, induced by the jet boundaries.

CONCLUSIONS

1. The method used in this investigation has made possible the experimental determination of jet boundary corrections for monoplane airfoils in open jets of four shapes for ratios of model span to jet width up to 0.75.

2. Prandtl's theoretical method of correcting for jet boundary effect in circular open throat tunnels may be considered satisfactory for monoplane airfoils whose span is not greater than 0.6 of the jet diameter.

3. The experimentally determined correction factors for angle of attack were, in general, greater than those for drag.

4. Jet boundaries had no appreciable effect on the airfoil pitching moments or center of pressure within the limits of the investigation.

5. Jet boundaries also had no appreciable effect on the pitching moments of a complete airplane.

6. Increasing turbulence appeared to increase the minimum drag and maximum lift, and to decrease the pitching moment.

LANGLEY MEMORIAL AERONAUTICAL LABORATORY,
NATIONAL ADVISORY COMMITTEE FOR AERONAUTICS,
LANGLEY FIELD, HAMPTON, VA.,
April 16, 1930.

REFERENCES

Reference 1. Warner, E. P.: Airplane Design, "Aerodynamics" (Ch. X, Scale Effect), pp. 162 to 183 (1926).

Reference 2. Dryden, H. L., and A. M. Kuethe: The Measurement of Fluctuations of Air Speed by the Hot-wire Anemometer. N. A. C. A. Technical Report No. 320 (1929).

Reference 3. Dryden, H. L., and A. M. Kuethe: Effects of Turbulence in Wind Tunnel Measurements. N. A. C. A. Technical Report No. 342 (1930).

Reference 4. Prandtl, L.: Applications of Modern Hydrodynamics to Aeronautics. N. A. C. A. Technical Report No. 116 (1925).

Reference 5. Wieselsberger, C.: Wind Tunnel Tests of Correction Formula for wings of Large Span. N. A. C. A. Technical Memorandum No. 263 (1924).

Reference 6. Glauert, H.: Aerofoil and Airscrew Theory (Ch. XIV, Wind Tunnel Interference on Aerofoils), pp. 189 to 198 (1926).

Reference 7. Jacobs, Eastman N.: Investigation of Airflow in Open-throat Wind Tunnels. N. A. C. A. Technical Report No. 322 (1929).

Reference 8. Reid, Elliott G.: Standardization of N. A. C. A. No. 1 Wind Tunnel. N. A. C. A. Technical Report No. 195 (1924).

Reference 9. Glauert, H.: The Effect of the Static Pressure Gradient on the Drag of a Body Tested in a Wind Tunnel. Reports and Memoranda No. 1158 (1928).

Reference 10. Wieselsberger, C.: The Improvement of Airflow in Wind Tunnels. Technical Memorandum No. 470 (1925).

Reference 11. Glauert, H.: Aerofoil and Airscrew Theory (Ch. X, The Aerofoil in Three Dimensions), pp. 125 to 136 (1926).

Reference 12. Eiffel, G., translated by Jerome C. Hunsaker: Resistance of the Air and Aviation (Ch. I), (1913).

APPENDIX

Balance alignment.

If the direction in which the lift is measured on a wind tunnel balance is not normal to the effective direction of the air stream over the airfoil, the angle of

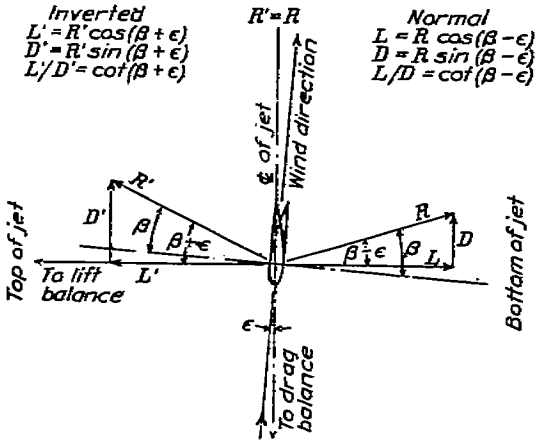

FIGURE 38.—Force diagram for alignment tests

attack, lift and drag as measured will be incorrect. This error may be eliminated by making two tests, one with the airfoil in the normal test position, and one with it inverted and averaging the results. It appears that this method was first used by Eiffel in 1910 (Reference 12).

It is not necessary to use this double test method in all tests if the balance is once properly aligned. This can be accomplished by making one set of airfoil tests in the normal and inverted positions, and calculating therefrom the amount by which the balance is misaligned. The balance system can then be adjusted and the results of tests with the airfoil in the normal position will be correct. An occasional check test will enable the proper alignment to be maintained.

A satisfactory method of determining the direction of the air stream involves the use of the values of maximum $\frac{L}{D}$ for both the normal and inverted test positions. If the center line of the wind tunnel jet be taken as a convenient arbitrary reference for initially aligning the balance system, the angle, ϵ, between this line and the effective wind direction will modify the measured lift and drag as shown in Figure 38. From the figure it will be seen that for the normal test position $\frac{L}{D}=\cot(\beta-\epsilon)$ and for the inverted position $\frac{L'}{D'}=\cot(\beta+\epsilon)$ $\left(\text{where } \beta=\cot^{-1}\frac{L}{D}\right)$. For the maximum values of $\frac{L}{D}$, β is a minimum and, therefore, the same for both positions, and

$$\epsilon=\frac{\cot^{-1}\left(\frac{L'}{D'}\right)\text{max.}-\cot^{-1}\left(\frac{L}{D}\right)\text{max.}}{2}.$$

A simple graphical method of obtaining ϵ when $\left(\frac{L}{D}\right)$max. and $\left(\frac{L'}{D'}\right)$max. are known is given in Figure 39, which is self-explanatory.

If the two $\frac{L}{D}$ curves are plotted against indicated angles of attack, a curve drawn through the mean values of the points will approximate the true $\frac{L}{D}$ curve. The error in maximum $\frac{L}{D}$ is then the difference between the maximum value of either of these curves and that of the mean curve. In addition, the angle which the lift members of the balance system make

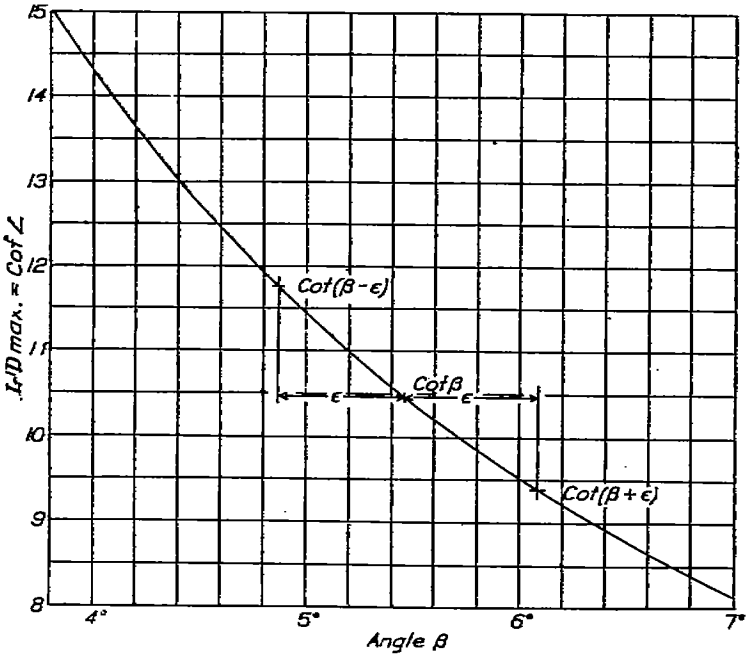

FIGURE 39.—Graphical method of obtaining the angle ε

with the normal to the effective air stream direction is approximately the difference between the angles at which $\frac{L}{D}=0$ for either experimental curve and the

mean curve. However, this simple method of obtaining the angle of deviation should be used only as a rough determination, since the experimental errors in setting the angle of attack are usually considerably larger than the maximum allowable deviation which, in general, should not be greater than ± 0.05 degree for airfoil tests. For accurate alignment, the method involving the use of maximum $\frac{L}{D}$ should be used as explained above. However, exceptional care should be taken in obtaining these maximum values of $\frac{L}{D}$.

In the foregoing investigation the accurate method was used in aligning the balance system in each jet.

Force tests were made on the airfoil in both normal and inverted positions, and the corresponding values of $\frac{L}{D}$ were obtained. The angle, ϵ, between the effective air stream direction and the center line was then determined on the basis of the differences in maximum $\frac{L}{D}$ for the two tests, and the direction of the lift wires was changed accordingly. This was most easily accomplished by multiplying sin ϵ by the weight used. The result represented the component which the drag balance should read when the weight was in place on the airfoil. The length of the drag wires was then adjusted until the tare with and without the weight

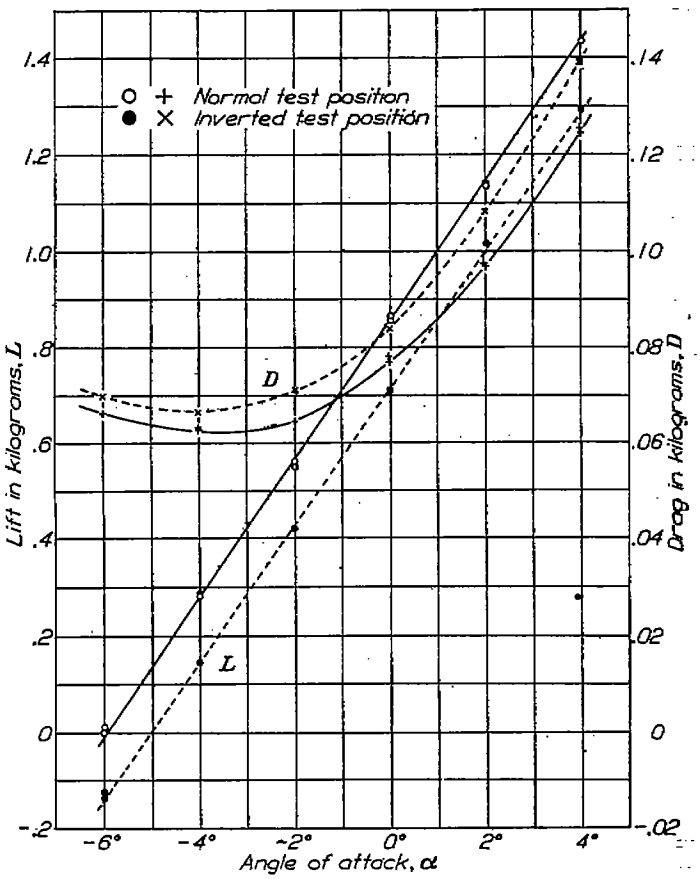

FIGURE 40.—Alignment force tests: Lift and drag versus angle of attack. Note: 4-inch by 20-inch Clark Y airfoil. q lb. 9.3 = per square foot

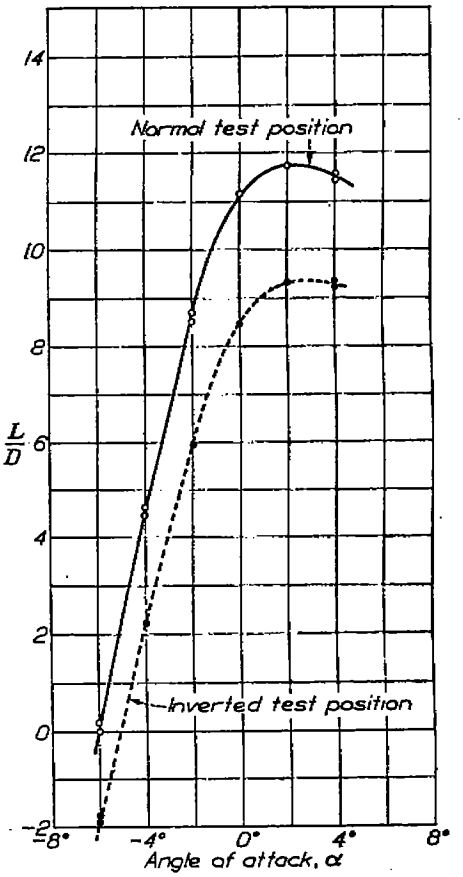

FIGURE 41.—Alignment force tests: L/D versus angle of attack

The 4-inch chord airfoil was mounted in the tunnel with a duplicate set of lugs on the upper surface. The center line of the jet was taken as the arbitrary base line. The length of the lift wires was first adjusted to bring the drag wires into the horizontal plane of the jet center line. The lift wires were then made perpendicular to the horizontal base line in the following manner: First, the tare drag was measured, then a weight was placed on the airfoil and the drag measured again. Any difference between the two readings was eliminated by changing the length of the drag wires, and thereby shifting the lift wires until the tare drag was the same with the weight either on or off.

differed by this amount. Since in these tests the forces were taken only over the angle of attack range from zero lift through maximum lift, it was not necessary to realign the drag wires because the drag forces were so small that the component in the lift direction was negligible. Figure 40 shows the measured lift and drag as obtained from the tests in the two positions plotted versus indicated angle of attack α. From the curves of $\frac{L}{D}$ versus α, Figure 41 the maximum values of $\frac{L}{D}$ were taken. These values are shown in Figure 39 as cot $(\beta-\epsilon)$ and cot $(\beta+\epsilon)$. This figure shows that

the angle, ϵ, in this particular case was 0.62 degree. The sense of this angle was as shown in Figure 38, so that to align the balance and airfoil with the wind direction the airfoil was moved upstream until the lift wires made an angle of 0.62 degree with the vertical. The difference in the tare drag readings with and without a 2,000-gram weight on the airfoil was:

$$\Delta D_T = 2{,}000 \sin 0.62 \text{ degree}$$

$$= 21.5 \text{ grams.}$$

The angle was such that the tare drag was greater with the weight in place.

In some wind tunnel installations it is not possible to align the balance with respect to the air stream. In this event, after the angle ϵ has been determined, the true drag may be obtained by correcting the measured drag in the following manner:

$$D = D' \pm L \sin \epsilon.$$

Whether the drag correction is to be added or subtracted from the measured drag depends, of course, on the sense of ϵ.

TABLE I.—FORCE TEST EFFECT OF TURBULENCE

($\sqrt{2}$ to 1 rectangular jet; 5-in. by 25-in. Clark Y airfoil)

Without screen					With screen				
α deg.	C_L	C_D	C_{D_s}	C_M	α deg.	C_L	C_D	C_{D_s}	C_M
−6	−0.036	0.0273	0.0272	−0.0713	−6	−0.031	0.0271	0.0270	−0.0654
−4	+.089	.0255	.0247	−.0674	−4	+.0947	.0262	.0253	−.0640
−2	.213	.0276	.0233	−.0650	−2	.2201	.0283	.0237	−.0613
0	.338	.0330	.0221	−.0647	0	.3395	.0335	.0225	−.0596
2	.470	.0425	.0214	−.0639					
4	.592	.0550	.0215	−.0643					
5					5	.6555	.0619	.0208	−.0599
6	.715	.0705	.0217	−.0646					
8	.835	.0894	.0229	−.0629					
10	.939	.1093	.0256	−.0659	10	.9345	.1087	.0254	−.0636
12	1.035	.1330	.0308	−.0673					
14	1.128	.1565	.0352	−.0677	14	1.131	.1564	.0333	−.0665
16	1.200	.1800	.0425	−.0681	16	1.211	.1812	.0412	−.0690
18	1.220	.2100	.0679	−.0743	18	1.257	.2136	.0628	−.0785
20	1.135	.2510	.1170	−.0888	20	1.246	.2550	.1068	−.0916

TABLE II.—FORCE TEST, CIRCULAR JET

(Data taken from faired curves for determination of δ_α)

C_L	$\frac{S}{A}=0$	3-in. by 15-in. airfoil			4-in. by 20-in. airfoil			5-in. by 25-in. airfoil		
	α_a deg.	α_a' deg.	$\Delta\alpha$	δ_α	α_a' deg.	$\Delta\alpha$	δ_α	α_a' deg.	$\Delta\alpha$	δ_α
0.1	1.42	1.45	0.03	0.102	1.48	0.06	0.115	1.57	0.15	0.133
.2	2.81	2.89	.08	.136	2.96	.15	.143	3.06	.25	.152
.3	4.20	4.32	.12	.136	4.41	.21	.134	4.62	.42	.170
.4	5.61	5.76	.15	.127	5.87	.26	.124	6.13	.52	.158
.5	7.00	7.19	.19	.129	7.32	.32	.122	7.68	.68	.166
.6	8.40	8.60	.20	.113	8.79	.39	.124	9.25	.85	.173
.7	9.80	10.08	.28	.136	10.29	.49	.134	10.86	1.06	.184
.8	11.27	11.57	.30	.127	11.81	.56	.129	12.49	1.22	.186
.9	12.79	13.12	.33	.125	13.45	.66	.139	14.18	1.39	.189
1.0	14.40	14.77	.37	.127	15.13	.73	.139	15.93	1.53	.187
1.1	16.13	16.58	.45	.139	17.01	.88	.153	17.90	1.77	.197
Av.				.127			.132			.177

*$\frac{S}{A}=0$ represents free air conditions.

TABLE III.—FORCE TEST, CIRCULAR JET

(Data taken from faired curves for determination of δ_D)

C_L	$\frac{S}{A}=0$	3-in. by 15-in. airfoil			4-in. by 20-in. airfoil			5-in. by 25-in. airfoil		
	C_D	C_D'	ΔC_D	δ_D	C_D'	ΔC_D	δ_D	C_D'	ΔC_D	δ_D
0.1		0.0259			0.0259			0.0259		
.2		.0270			.0270			.0270		
.3	0.0281	.0288	0.0007	0.151	.0293	0.0012	0.146	.0297	0.0016	0.124
.4	.0320	.0333	.0013	.157	.0342	.0022	.150	.0351	.0031	.135
.5	.0381	.0396	.0015	.116	.0406	.0024	.105	.0433	.0052	.145
.6	.0446	.0470	.0024	.129	.0491	.0045	.136	.0530	.0084	.163
.7	.0539	.0569	.0030	.119	.0592	.0060	.133	.0641	.0102	.146
.8	.0643	.0684	.0041	.124	.0717	.0074	.126	.0773	.0130	.142
.9	.0766	.0816	.0050	.120	.0855	.0089	.120	.0927	.0161	.139
1.0	.0905	.0967	.0062	.120	.1014	.0109	.119	.1102	.0197	.133
1.1	.1067	.1149	.0082	.131	.1212	.0145	.131	.1308	.0241	.139
1.2	.1315	.1420	.0105	.141	.1503	.0188	.143	.1600	.0285	.138
Av.				.125			.127			.142

*$\frac{S}{A}=0$ represents free air conditions.

TABLE IV.—CORRECTION FACTORS

$$\delta_D = \frac{\Delta C_{D_i}}{C_L^2 \frac{S}{A}} \qquad \delta_\alpha = \frac{\Delta \alpha_i}{C_L \frac{S}{A} \frac{180}{\pi}}$$

Jet shape	3-in. by 15-in. airfoil		4-in. by 20-in. airfoil		5-in. by 25-in airfoil	
	δ_D	δ_α	δ_D	δ_α	δ_D	δ_α
Circular jet:						
Theoretical	0.126	0.126	0.128	0.128	0.132	0.132
Experimental	.125	.127	.127	.132	.142	.177
2 to 1 circular side jet	.235	.386	.215	.272	.196	.239
$\sqrt{2}$ to 1 circular side jet	.170	.249	.160	.193	.164	.194
$\sqrt{2}$ to 1 rectangular jet	.210	.301	.206	.201	.200	.222

TABLE V.—FORCE TEST, CIRCULAR JET

(3-in. by 15-in. Clark Y airfoil)

α_a' deg.	C_D'	C_L	C_M	C_p	C_D	α_a deg.
−0.60	0.0252	−0.040	−0.0725	−1.553	0.0252	−0.59
+1.45	.0241	+.099	−.0709	+.967	.0240	+1.41
3.47	.0260	.238	−.0676	.534	.0256	3.38
5.51	.0311	.384	−.0663	.422	.0301	5.37
7.55	.0399	.527	−.0662	.376	.0381	7.35
9.59	.0519	.667	−.0637	.346	.0490	9.34
11.63	.0672	.806	−.0653	.331	.0632	11.33
13.67	.0850	.934	−.0654	.320	.0793	13.33
15.70	.1044	1.052	−.0677	.314	.0973	15.31
17.73	.1267	1.158	−.0663	.307	.1183	17.30
19.75	.1529	1.227	−.0654	.303	.1432	19.30
21.75	.1839	1.219	−.0602	.316	.1744	21.30
23.75	.2229	1.190	−.1013	.335	.2138	23.30
25.72	.2702	1.133	−.1100	.347	.2611	25.10

TABLE VI.—FORCE TEST, CIRCULAR JET

(4-in. by 20-in. Clark Y airfoil)

α_a' deg.	C_D'	C_L	C_M	C_p	C_D	α_a deg.
−0.50	0.0261	−0.036	−0.0715	−1.735	0.0261	−0.48
+1.52	.0241	+.102	−.0674	+.910	.0241	+1.45
3.54	.0260	.239	−.0645	.520	.0253	3.33
5.56	.0309	.388	−.0641	.415	.0292	5.31
7.38	.0397	.516	−.0656	.377	.0367	7.24
9.60	.0523	.656	−.0653	.349	.0474	9.17
11.62	.0677	.786	−.0658	.334	.0608	11.11
13.64	.0848	.911	−.0661	.323	.0763	13.04
15.66	.1053	1.028	−.0683	.316	.0933	14.99
17.68	.1278	1.132	−.0695	.311	.1126	16.94
19.69	.1523	1.212	−.0709	.308	.1355	18.89
21.69	.1843	1.210	−.0803	.316	.1676	20.89
23.69	.2218	1.180	−.0892	.326	.2069	22.92
25.68	.2603	1.126	−.1025	.341	.2458	24.94

TABLE VII.—FORCE TEST, CIRCULAR JET

(5-in. by 25-in. Clark Y airfoil)

α_s' deg.	C_D'	C_L	C_M	C_p	C_D	α_s deg.
−.48	0.0251	−0.028	−0.0718	−1.381	0.0251	−0.44
+1.52	.0241	+.099	−.0691	+.949	.0239	+1.38
3.54	.0254	.235	−.0669	.535	.0243	3.20
5.56	.0308	.368	−.0659	.429	.0280	5.02
7.57	.0411	.500	−.0679	.386	.0362	6.84
9.59	.0580	.624	−.0674	.358	.0448	8.68
11.60	.0672	.744	−.0683	.343	.0560	10.53
13.61	.0848	.865	−.0667	.327	.0696	12.36
15.62	.1052	.985	−.0679	.319	.0860	14.19
17.63	.1262	1.085	−.0691	.314	.1040	16.06
19.64	.1512	1.185	−.0706	.310	.1227	17.92
21.65	.1752	1.234	−.0708	.307	.1442	19.86
23.65	.2112	1.230	−.0823	.318	.1806	21.87
25.64	.2492	1.195	−.0981	.332	.2221	23.94

TABLE VIII.—FORCE TEST

($\sqrt{2}$ to 1 rectangular jet; 3-in. by 15-in. Clark Y airfoil)

α_s' deg.	C_D'	C_L	C_M	C_p	C_D	α_s deg.
−0.65	0.0271	−0.041	−0.0712	−1.513	0.0271	−0.61
+1.38	.0241	.092	−.0677	+.985	.0241	+1.29
3.42	.0259	.237	−.0641	.533	.0253	3.20
5.45	.0305	.385	−.0639	.425	.0295	5.09
7.50	.0392	.505	−.0616	.372	.0364	7.00
9.54	.0515	.643	−.0602	.344	.0467	8.91
11.57	.0665	.771	−.0607	.329	.0595	10.81
13.61	.0838	.904	−.0604	.317	.0741	12.72
15.64	.1035	1.013	−.0637	.318	.0911	14.64
17.67	.1243	1.110	−.0628	.307	.1090	16.58
19.69	.1475	1.179	−.0604	.301	.1309	18.53
21.69	.1843	1.190	−.0744	.312	.1673	20.52
23.69	.2293	1.165	−.0926	.330	.2130	22.55
25.67	.2630	1.095	−.1038	.345	.2486	24.59

TABLE IX.—FORCE TEST

($\sqrt{2}$ to 1 rectangular jet; 4-in. by 20-in. Clark Y airfoil)

α_s' deg.	C_D'	C_L	C_M	C_p	C_D	α_s deg.
−0.63	0.0253	−0.038	−0.0720	−1.645	0.0253	−0.59
+1.39	.0241	+.094	−.0686	+.980	.0239	+1.28
3.41	.0263	.222	−.0654	.545	.0252	3.15
5.43	.0314	.355	−.0645	.432	.0288	5.02
7.45	.0401	.492	−.0646	.381	.0351	6.87
9.47	.0527	.620	−.0654	.355	.0446	8.75
11.49	.0689	.750	−.0671	.340	.0571	10.61
13.51	.0879	.875	−.0689	.329	.0719	12.49
15.53	.1062	.993	−.0688	.319	.0876	14.37
17.54	.1304	1.095	−.0678	.312	.1053	16.26
19.56	.1534	1.173	−.0697	.309	.1244	18.19
21.56	.1874	1.185	−.0815	.319	.1581	20.18
23.55	.2224	1.160	−.0895	.327	.1943	22.19
25.55	.2584	1.108	−.1039	.344	.2328	24.26

TABLE X.—FORCE TEST

($\sqrt{2}$ to 1 rectangular jet; 5-in. by 25-in. Clark Y airfoil)

α_s' deg.	C_D'	C_L	C_M	C_p	C_D	α_s deg.
−0.60	0.0259	−0.036	−0.0713	−1.729	0.0260	−0.53
+1.41	.0241	+.089	−.0674	+1.007	.0240	+1.23
3.42	.0262	.213	−.0650	.555	.0249	2.99
5.44	.0314	.338	−.0647	.442	.0280	4.76
7.45	.0411	.470	−.0639	.386	.0343	6.59
9.46	.0536	.592	−.0643	.359	.0426	8.27
11.47	.0691	.715	−.0646	.340	.0531	10.03
13.49	.0880	.836	−.0629	.326	.0661	11.81
15.50	.1084	.939	−.0659	.320	.0806	13.61
17.51	.1316	1.035	−.0673	.315	.0982	15.43
19.52	.1551	1.128	−.0677	.310	.1148	17.25
21.53	.1786	1.200	−.0681	.307	.1327	19.11
23.53	.2086	1.220	−.0743	.311	.1617	21.07
25.52	.2496	1.185	−.0888	.325	.2053	23.13

TABLE XI.—FORCE TEST

($\sqrt{2}$ to 1 circular side jet; 3-in. by 15-in. Clark Y airfoil)

α_s' deg.	C_D'	C_L	C_M	C_p	C_D	α_s deg.
−0.60	0.0256	−0.037	−0.0730	−1.720	0.0256	−0.56
+1.43	.0241	+.096	−.0691	+.970	.0240	+1.34
3.47	.0254	.232	−.0651	.531	.0245	3.24
5.51	.0300	.373	−.0642	.422	.0296	5.16
7.55	.0384	.512	−.0631	.378	.0366	7.06
9.59	.0511	.641	−.0626	.348	.0466	8.98
11.62	.0667	.773	−.0635	.332	.0599	10.91
13.66	.0853	.905	−.0631	.320	.0739	12.80
15.69	.1039	1.022	−.0648	.313	.0923	14.76
17.73	.1264	1.125	−.0636	.307	.1110	16.66
19.74	.1460	1.190	−.0629	.303	.1298	18.60
21.74	.1855	1.190	−.0781	.313	.1653	20.60
23.73	.2296	1.160	−.0912	.329	.2134	22.62
25.72	.2661	1.108	−.1039	.344	.2620	24.66

TABLE XII.—FORCE TEST

($\sqrt{2}$ to 1 circular side jet; 4-in. by 20-in. Clark Y airfoil)

α_s' deg.	C_D'	C_L	C_M	C_p	C_D	α_s deg.
−0.52	0.0253	−0.031	−0.0718	−2.060	0.0258	−0.48
+1.49	.0241	+.096	−.0673	+.950	.0239	+1.36
3.52	.0255	.230	−.0656	.536	.0245	3.22
5.54	.0299	.360	−.0646	.430	.0275	5.06
7.56	.0400	.495	−.0658	.383	.0355	6.91
9.58	.0526	.623	−.0664	.356	.0452	8.76
11.60	.0683	.755	−.0666	.338	.0574	10.60
13.62	.0865	.879	−.0672	.321	.0717	12.45
15.64	.1071	.998	−.0684	.319	.0880	14.33
17.65	.1293	1.106	−.0696	.313	.1059	16.19
19.67	.1521	1.182	−.0686	.308	.1252	18.11
21.67	.1851	1.182	−.0779	.316	.1533	20.11
23.66	.2191	1.170	−.0836	.321	.1931	22.11
25.65	.2581	1.120	−.1008	.340	.2341	24.18

TABLE XIII.—FORCE TEST

($\sqrt{2}$ to 1 circular side jet; 5-in. by 25-in. Clark Y airfoil)

α_s' deg.	C_D'	C_L	C_M	C_p	C_D	α_s deg.
−0.52	0.0259	−0.031	−0.0710	−2.040	0.0259	−0.46
+1.49	.0241	+.090	−.0678	+1.004	.0239	+1.30
3.50	.0256	.224	−.0653	.541	.0241	3.04
5.52	.0302	.343	−.0636	.435	.0263	4.81
7.53	.0402	.470	−.0656	.390	.0331	6.56
9.54	.0521	.595	−.0646	.359	.0409	8.32
11.55	.0675	.710	−.0652	.342	.0521	10.07
13.57	.0949	.826	−.0646	.328	.0640	11.87
15.58	.1059	.936	−.0653	.320	.0793	13.66
17.59	.1281	1.038	−.0666	.314	.0949	15.45
19.60	.1519	1.132	−.0673	.309	.1126	17.26
21.61	.1754	1.200	−.0660	.306	.1312	19.12
23.59	.1999	1.208	−.1019	.334	.1642	21.11

TABLE XIV.—FORCE TEST

(2 to 1 circular side jet; 3-in. by 15-in. Clark Y airfoil)

α_s' deg.	C_D'	C_L	C_M	C_p	C_D	α_s deg.
−0.45	0.0255	−0.028	−0.0701	−2.555	0.0255	−0.39
+1.59	.0241	+.098	−.0667	+.931	.0239	+1.39
3.61	.0259	.224	−.0631	.532	.0248	3.16
5.65	.0308	.350	−.0607	.424	.0281	4.95
7.69	.0395	.484	−.0621	.378	.0345	6.73
9.72	.0520	.613	−.0597	.347	.0439	8.49
11.76	.0665	.739	−.0594	.330	.0557	10.28
13.79	.0843	.859	−.0597	.320	.0686	12.07
15.83	.1050	.971	−.0618	.314	.0846	13.89
17.85	.1269	1.070	−.0610	.307	.1004	15.71
19.88	.1489	1.150	−.0599	.302	.1207	17.68
21.88	.1765	1.183	−.0657	.306	.1466	19.51
23.88	.2160	1.165	−.0902	.319	.1870	21.55
25.86	.2570	1.105	−.0949	.336	.2309	23.65

TABLE XV.—FORCE TEST

(2 to 1 circular side jet; 4-in. by 20-in. Clark Y airfoil)

α_a' deg.	$C_{D'}$	C_L	C_M	C_y	C_D	α_a deg.
−0.55	0.0257	−0.029	−0.0719	−2.225	0.0257	−0.48
+1.46	.0241	+0.094	−.0675	+0.963	.0238	+1.22
3.48	.0261	.214	−.0652	.554	.0244	2.94
5.50	.0310	.337	−.0627	.436	.0270	4.65
7.52	.0408	.467	−.0634	.385	.0333	6.35
9.54	.0535	.583	−.0634	.358	.0416	8.06
11.56	.0694	.709	−.0629	.339	.0520	9.78
13.58	.0879	.822	−.0635	.327	.0645	11.52
15.60	.1093	.930	−.0639	.319	.0794	13.26
17.61	.1318	1.032	−.0646	.313	.0949	15.01
19.62	.1558	1.123	−.0648	.308	.1121	16.80
21.63	.1843	1.162	−.0703	.311	.1374	18.71
23.63	.2188	1.145	−.0795	.319	.1784	20.75
25.62	.2543	1.098	−.0901	.332	.2128	22.56

TABLE XVI.—FORCE TEST

(2 to 1 circular side jet; 5-in. by 25-in. Clark Y airfoil)

α_a' deg.	$C_{D'}$	C_L	C_M	C_y	C_D	α_a deg.
−0.45	0.0261	−0.026	−0.0719	−2.510	0.0261	−0.36
+1.56	.0241	+.092	−.0673	+.982	.0237	+1.25
3.57	.0260	.204	−.0637	.562	.0239	2.86
5.58	.0311	.319	−.0619	.444	.0261	4.47
7.60	.0406	.444	−.0638	.394	.0310	6.07
9.61	.0532	.554	−.0627	.362	.0381	7.69
11.62	.0685	.666	−.0617	.343	.0467	9.32
13.63	.0870	.774	−.0619	.330	.0575	10.97
15.64	.1083	.873	−.0630	.322	.0709	12.63
17.65	.1305	.962	−.0637	.316	.0847	14.34
19.66	.1553	1.055	−.0632	.310	.1006	16.03
21.67	.1800	1.132	−.0624	.305	.1172	17.76
23.67	.2025	1.190	−.0593	.300	.1327	19.56
25.67	.2345	1.170	−.0727	.312	.1674	21.65

TABLE XVII.—FORCE TEST, CIRCULAR JET

(T. S. seaplane model)

α_a' deg.	C_L	C_M	α_a' deg.	C_L	C_M
−0.80	−0.046	+0.1220	13.20	0.781	−0.0272
+1.20	+.071	.1120	15.20	.878	−.0655
3.20	.185	.0992	17.20	.988	−.1170
5.20	.312	.0872	19.20	1.064	−.1630
7.20	.442	.0639	21.20	1.161	−.202
9.20	.554	.0425	23.20	1.141	−.246
11.20	.664	.0094	25.20	1.098	−.298

TABLE XVIII.—FORCE TEST

($\sqrt{2}$ to 1 rectangular jet; T. S. seaplane model)

α_a' deg.	C_L	C_M	α_a' deg.	C_L	C_M
−0.24	−0.007	+0.1185	13.76	0.730	−0.0168
+1.76	+.095	.1126	15.76	.835	−.0564
3.76	.198	.1062	17.76	.930	−.0956
5.76	.312	.0940	19.76	1.021	−.1400
7.76	.425	.0738	21.76	1.099	−.1805
9.76	.529		23.76	1.090	−.2170
11.76	.631	.0175			

TABLE XIX.—FORCE TEST

($\sqrt{2}$ to 1 circular side jet; T. S. seaplane model)

α_a' deg.	C_L	C_M	α_a' deg.	C_L	C_M
−0.60	−0.018	+0.126	13.40	0.703	−0.0028
+1.40	+.080	.120	15.40	.807	−.0376
3.40	.178	.111	17.40	.895	−.0774
5.40	.290	.0978	19.40	.980	−.1211
7.40	.407	.0796	21.40	1.058	−.1655
9.40	.512	.0570	23.40	1.080	−.2070
11.40	.602	.0252	25.40	1.032	−.235

TABLE XX.—FORCE TEST

(2 to 1 circular side jet; T. S. seaplane model)

α_a' deg.	C_L	C_M	α_a' deg.	C_L	C_M
−0.24	−0.002	+0.1275	13.76	0.615	0.0432
+1.76	+.084	.1260	15.76	.690	.0176
3.76	.173	.1230	17.76	.753	−.0109
5.76	.264	.1139	19.76	.824	−.0421
7.76	.368	.1010	21.76	.897	−.0759
9.76	.455	.0849	23.76	.955	−.116
11.76	.535	.0656	25.76	.974	−.165